



**Mechanical properties of friction stir processed TIG-welded and
friction stir welded 5083 aluminium alloy joints.**

By

Sipokazi Mabuwa

Thesis submitted in fulfilment of the requirements for the degree

Master of Engineering: Mechanical Engineering

in the Faculty of Engineering

at the Cape Peninsula University of Technology

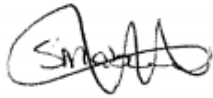
Supervisor: Dr Velaphi Msomi

Bellville

March 2019

DECLARATION

I, Sipokazi Mabuwa, declare that the contents of this thesis represent my own unaided work, and that the thesis has not previously been submitted for academic examination towards any qualification. Furthermore, it represents my own opinions and not necessarily those of the Cape Peninsula University of Technology.



25/03/2019

Signed

Date

ABSTRACT

Material processing is all about improving the materials that already exist, discovering new ones, and finding original ways to use existing materials to produce high-quality, cost-effective parts and systems. It is very evident from day to day life that everyday technology keeps changing for better, to make life easier and simpler. As the technology keeps on evolving, manufacturers and designers will be at ease knowing that quality is not compromised. Friction stir processing is one of the new material processing techniques, derived from friction stir welding.

The aim of this study was to characterize the mechanical behaviour of friction stir processed TIG welded 5083 aluminium plate and friction stir processed FSW 5083 aluminium plate as compared to unprocessed friction stir welded 5083 aluminium plate and TIG welded plate. Prior to the analysis of the plates, two 5083 aluminium alloy plates were welded using the two different welding techniques i.e. friction stir welding and Tungsten Inert Gas welding (TIG). The welded joints were then friction stir processed (FSP) using the parameters used during the FSW. The friction stir processed (or processed) joints were then cut and prepared for different analysis. This involved the tensile tests, bending tests, hardness tests, macrostructure and microstructure analysis. These analyses were performed so as to study the impact of applying the FSP on the previously mentioned joints (FSW and TIG welded joints).

The unprocessed TIG welded joints were found to be the weakest joints amongst all the joints studied in this work. The processed FSW joints were found to be the strongest amongst the joints studied in this work. The characterized specimens were cut from different locations of the plates i.e. the beginning, the middle and the end of the plate. The specimens were also symbolized in a way representing their cut locations (A for the beginning, B for the middle and C for the end of the plate). This then suggests that each plate produced three specimens. It was noted that the behaviour of the unprocessed TIG welded joint was uniform along with the plate while the other joints vary with location. The specimens cut at the beginning of the plates were found to be weaker compared to the one cut in the middle and the end of the plates. This trend was noted on the processed TIG welded joints, unprocessed FSW and processed FSW welded joints. The results showed a clear distinction between processed joints and unprocessed joints. There was a good correlation observed between the microstructural results, bending and the tensile

results. Refined grains were also observed on the microstructure of the processed weld joints. It was noticed that the hardness value of the processed joints was higher compared to that of the base material. The detailed correlation between the microstructure and the macrostructure is reported in the main text.

ACKNOWLEDGEMENTS

To God be the glory!

I would like to express my sincere gratitude to my supervisor Dr. Velaphi Msomi for his guidance, motivation and patience and most of all for having faith in in me to carry out this research. It has been an honour working under your wing.

I would like to express my gratitude to the mechanical engineering department workshop technical staff for their help, especially Molebogeng Segaletsho and Shaheeda Petersen. Not forgetting Busch Ricardo from the Adaptronics Advanced Manufacturing Technology Laboratory. My special gratitude also goes to electron microscope unit, physics department at the University of the Western Cape.

CPUT, for paying my tuition fees, I highly appreciate it.

I would also like to thank my husband Zanoxolo Mabuwa for allowing me to study further to this level. Thank you so much Manci for being there throughout the process, and for all your helping every way possible.

To my kids Isipho Angela, Esihle Samuel, and Qhawe Kamva you have been my inspiration.

Special appreciation to my sisters in-law Anelisa and Nomfundiso Mabuwa for babysitting my kids when I had to study.

Special thanks to my maternal Family (Ngalo), for the love and moral support.

TABLE OF CONTENTS

Contents

Table of Contents

DECLARATION	2
ABSTRACT	3
ACKNOWLEDGEMENTS	5
TABLE OF CONTENTS	6
LIST OF FIGURES	9
LIST OF TABLES	12
GLOSARY	13
CHAPTER ONE	15
INTRODUCTION	15
1.1 Problem Statement	19
1.1.1 Tungsten Inert Gas Welding	16
1.1.2 Friction Stir Welding	17
1.1.3 Friction Stir Processing	18
1.2 Research Background	19
1.3 Research Objectives	20
1.4 Review of Related Literature	21
1.5 Dissertation Outline	22
CHAPTER TWO	23
LITERATURE REVIEW	23
2.1. Friction Stir Welding	23
2.2 FSW of Aluminium Alloys	24
2.3 TIG Welding of Aluminium alloys	25
2.4 FSP of Aluminium Alloys	27
2.5 Summary	30
CHAPTER THREE	31
EXPERIMENTAL SETUP AND PERFORMANCE	31
3.1 Welding Setup	31
3.1.1 Guillotine Shear Master Cutting Machine	31
3.1.2 TIG Welding Equipment	32
3.1.3 Friction Stir Welding Machine	33
3.2 Welding Performance	33
3.2.1 TIG Process	34
3.2.2 Friction Stir Welding	34
3.2.3 Friction Stir Processing	36

3.3 Weldments Analysis Preparation	38
3.3.1 EDM Wire Cut Accutex AU-5001A Machine	38
3.3.2 Struers Labopress-3 Mounting Press Machine.....	39
3.3.3 Struers LaboPol-5 polishing machine	40
3.4 Performance of Specimen Preparation	41
3.4.1 Tensile Tests Specimen Preparation	41
3.4.2 Bending Tests Specimen Preparations.....	42
3.4.3 Microstructural Tests Specimen Preparation	42
3.4.4 Hardness Tests Specimens.....	44
3.5 List of Test Performed.....	44
3.6 Mechanical Tests.....	45
3.6.1 Tensile Test.....	45
3.6.2 Bending Test.....	47
3.6.3 Hardness Tester	49
3.6.4 Microstructural Tests	50
3.6.5 Scanning Electron Microscopy (SEM) Tests.....	50
CHAPTER FOUR.....	51
RESULTS AND DISCUSSIONS	51
4.1 Bending Tests	51
4.1.1 Processed and Unprocessed TIG results.....	52
4.1.2 Processed and unprocessed FSW results	56
4.2 Tensile Tests	61
4.2.1 Processed and Unprocessed TIG results.....	61
4.2.2 Processed and Unprocessed FSW	64
4.3 Hardness Tests.....	65
4.4 Macrostructure Tests	67
4.5 Microstructure Tests.....	69
4.6 Scanning Electron Microscopy (SEM) Tests	71
4.7 Comparison of Mechanical Properties	73
CHAPTER FIVE	75
CONCLUSIONS	75
RECOMMENDATIONS	76
APPENDICES	86
APPENDIX A	87
Aluminium Plate.....	87
APPENDIX B	88
Pin Drawing.....	88
APPENDIX C1	89
Tensile Test Specimen.....	89
APPENDIX C2	90

ASTM E8 Standard	90
APPENDIX D	91
ASTM E290-14	91
APPENDIX D2	93
Bending Specimen	93
APPENDIX E	94
Hardness Test Specimen.....	94
APPENDIX F.....	95
SAMPLE OF CALCULATIONS	95
Strain and Percentage Elongation	96
Maximum Shear Stress	96
Tensile Test Calculations	98
Ultimate Tensile Stress	98
Strain and Percentage Elongation	99
Yield Stress	100

LIST OF FIGURES

Figure 1: Schematic diagram of FSP setup and rotating tool [Sun, 2009]	3
Figure 3.1.1: Guillotine shear master cutting machine.....	16
Figure 3.1.2: TIG welding machine.....	16
Figure 3.1.3: FSW machine.....	17
Figure 3.2: Aluminium set of plates used.....	17
Figure 3.2.1: TIG welded plate.....	18
Figure 3.2.2: (a) FSW process.....	19
Figure 3.2.2: (b) Pin dimensions in mm.....	19
Figure 3.2.2: (c) FSW plate.....	20
Figure 3.2.3: (a) FSP application on FSW welded joint.....	21
Figure 3.2.3: (b) Processed FSW plate.....	21
Figure 3.2.3: (c) FSP application on TIG plate setup.....	21
Figure 3.2.3: (d) Processed TIG joint plate.....	22
Figure 3.3.1: Wire cut machine.....	23
Figure 3.3.2: Mounting press machine.....	24
Figure 3.3.3: Polishing machine.....	24
Figure 3.4.1: (a) Tensile test specimen with dimensions.....	25
Figure 3.4.1: (b) Sample of a tensile test specimen.....	25
Figure 3.4.2: (a) Bending test specimen with dimensions in mm.....	26
Figure 3.4.2: (b) Sample of a bending specimen.....	26
Figure 3.4.3: (a) Overall dimensioned microstructure test specimen.....	27
Figure 3.4.3: (b) Wire cut microstructure specimen samples.....	27
Figure 3.4.3: (c) Mounted microstructure test specimen samples.....	27
Figure 3.4.3: (d) Polished specimen samples.....	27
Figure 3.4.3: (e) Etched specimen sample specimens.....	28
Figure 3.4.4: Hardness test sample specimens.....	28
Figure 3.6.1: (a) Hounsfield machine.....	30
Figure 3.6.1: (b) Tensile testing flat jaws.....	30
Figure 3.6.2: (a) Bending test setup and apparatus.....	32
Figure 3.6.2: (b) Bending test schematic diagram.....	33
Figure 3.6.3: Hardness test machine.....	33
Figure 3.6.4: Microstructure apparatus.....	34
Figure 4.1: Sample specimen format.....	35

Figure 4.1.1: (a) Bended unprocessed TIG specimen.....	36
Figure 4.1.1: (b) Friction stir processed TIG (face) joints.....	36
Figure 4.1.1: (c) Friction stir processed TIG, bended (root) specimens.....	37
Figure 4.1.1: (d) Bending stress – strain curves for processed and unprocessed TIG (Face).....	38
Figure 4.1.1: (e) Bending stress – strain curves for processed and unprocessed TIG (Root).....	39
Figure 4.1.2: (a) FSW (face), bended specimens.....	41
Figure 4.1.2: (b) FSW (root) bended specimens.....	41
Figure 4.1.2: (c) Processed FSW (face), bended specimens.....	42
Figure 4.1.2: (d) Processed FSW (root) bended specimens.....	42
Figure 4.1.2: (e) Bending stress – strain curves for processed and unprocessed FSW (Face).....	43
Figure 4.1.2: (f) Bending stress – strain curves for processed and unprocessed FSW (Root).....	44
Figure 4.2.1: (a) Post-test TIG specimen.....	46
Figure 4.2.1: (b) Post-test FSP-TIG specimen.....	46
Figure 4.2.1: (c) Tensile stress – strain curves for processed and unprocessed TIG ...	47
Figure 4.2.2: (a) Post-test unprocessed FSW specimen.....	48
Figure 4.2.2: (b) Post-test FSP-FSW specimen.....	48
Figure 4.2.2: (c) Tensile stress – strain curves for processed and unprocessed FSW....	49
Figure 4.3: Hardness test post-test specimen samples.....	51
Figure 4.4.1: Unprocessed TIG welded 5083 alloy.....	52
Figure 4.4.2: Processed TIG alloy macrostructure - onion ring.....	52
Figure 4.4.3: Unprocessed FSW joints.....	53
Figure 4.4.4: Processed FSW onion ring.....	53
Figure 4.5.1: TIG Welded microstructure.....	54
Figure 4.5.2: Processed TIG alloy microstructure, nugget zone.....	55
Figure 4.5.3: FSW microstructure; nugget zone.....	55
Figure 4.5.4: Processed FSW Alloy Microstructure; nugget zone.....	56
Figure 4.6.1: Fracture surfaces.....	57
Figure 4.6.2: SEM Specimens; (a) Unprocessed FSW; (b) Unprocessed TIG; (c) Processed FSW; (d) Processed TIG.....	58
Figure 4.6.3: SEM Photos; (a) TIG, and (b) FSP-TIG.....	59
Figure 4.6.3: SEM Photos; (c) FSW, and (d) FSP-FSW.....	59

Figure A1: Aluminium plate.....	70
Figure B1: Pin.....	71
Figure C1: Dog Bone specimen.....	72
Figure C2: Bending specimen.....	76
Figure E1: Welding joint.....	77

LIST OF TABLES

Table 3.2.1: FSW parameters	20
Table 3.6.1: Tensile test parameters.	29
Table 4.1.1: Processed and unprocessed TIG bending results.	40
Table 4.1.2: Processed and unprocessed FSW bending results.	45
Table 4.2.1: Processed and unprocessed TIG tensile weld joints results.	48
Table 4.2.2: Processed and unprocessed FSW tensile weld joints results.	50
Table 4.3.1: Hardness test results.	52
Table 4.5.1: Grain sizes measured.	61
Table 4.7: Practical mechanical properties.	64

GLOSARY

Terms/Acronyms/Abbreviations	Definition/Explanation
CPUT	Cape Peninsula University of Technology
FSW	Friction Stir Welding
FSP	Friction Stir Processing
TIG	Tungsten Inert Gas
TWI	The Welding Institute
ASTM	American Society for Testing and Materials
TMAZ	Thermo-Mechanically Affected Zone
NZ	Nugget Zone
Cu	Copper
Al	Aluminium
Zn	Zinc
Mg	Magnesium
Si	Silicon
Li	Lithium
HAZ	The Heat Affected Zone
BM	Base Material
WM	Weld Metal
SEM	Scanning Electron Microscope
GMAW	Gas Metal Arc Welding
IOM	Orientation Imaging microscopy
UFG	Ultrafine Grain

HRB

Hardness Rockwell, B scale

EDM

Electro Discharge Machining

CHAPTER ONE

INTRODUCTION

1.1 Introduction

Aluminium and its alloys are used in many fields, whether in daily life or industrially. The reasons why aluminium and its alloys are common use is because they have low density, easy to work with, high electrical conductivity and high heat conductivity [Cevik et al., 2012]. Among the most striking characteristics of aluminium is its versatility. More than 300 alloy compositions are commonly recognized, and many additional variations have been developed worldwide. The most outstanding features which makes aluminium the most economical and attractive metal for various applications are appearance, fabricability, physical properties, mechanical properties and corrosion resistance [Totten & Mackenzie, 2003].

Aluminium alloys are divided into two major categories namely cast compositions and wrought compositions. The casting compositions are recognised by a three-digit system followed by a decimal value. The decimal .0 in all cases relates to casting alloy limits. Decimals .1, and .2 are ingot compositions, which after melting and processing should result in chemistries conforming to casting specification requirements. The cast categories include the 2xx.x series (Al-Cu), the 3xx.x series (Al-Si + Cu or Mg), the 4xx.x series (Al-Si), the 5xx.x series (Al-Mg), the 7xx.x series (Al-Zn), and the 8xx.x series (Al-Sn). The 2xx.x, 3xx.x, 7xx.x, and 8xx.x alloys can be strengthened by precipitation hardening, but the properties obtained are not as high as for the wrought heat treatable alloys [Park, 2015].

The wrought aluminium alloys are divided into heat treatable and non-heat treatable alloys. Wrought heat treatable alloys can be precipitation hardened to develop quite high strength levels. These alloys include the 2xxx series (Al-Cu and Al-Cu-Mg), the 6xxx series (Al-Mg-Si), the 7xxx series (Al-Zn-Mg and Al-Zn-Mg-Cu), and the aluminium-lithium alloys of the 8xxx alloy series. The 2xxx and 7xxx alloys, which develop the highest strength levels, are the main alloys used for metallic aircraft structure. The wrought non-heat-treatable alloys cannot be strengthened by precipitation hardening; they are hardened primarily by cold working. The wrought non-heat-treatable alloys

include the commercially pure aluminium series (1xxx), the aluminium-manganese series (3xxx), the aluminium-silicon series (4xxx), and the aluminium-magnesium series (5xxx). While some of the 4xxx alloys can be hardened by heat treatment, others can only be hardened by cold working [Davis, 2001].

The 5083-H111 aluminium alloy, from the wrought alloy 5xxx series, was selected to be utilized in this study. Generally, the 5xxx offer outstanding corrosion resistance, making them suitable for marine applications. The 5083 alloy has the highest strength of the non-heat treatable alloys but is not recommended for use in temperatures exceeding 65°C. The alloy is highly resistant to be attacked by both seawater and industrial chemical environments [Totten & Mackenzie, 2003]. Alloy 5083 also retains exceptional strength after welding in comparison to other alloys. The use of high strength aluminium alloys in the shipbuilding is increasing. The benefit of using aluminium material in building structures is the fact that aluminium is lighter in weight which contributes to the reduction of power consumption while increasing the cargo capacity. In as much as using aluminium for structures is beneficial, there are very limited techniques available used to join aluminium alloys. The most used technique includes Tungsten Inert Gas welding (TIG) and the emerging one called Friction Stir Welding.

1.1.1 Tungsten Inert Gas Welding

Tungsten inert gas welding by definition is a welding method that uses a tungsten electrode and a filler rod to weld metals together [Cetinel and Mehmet, 2014]. TIG welding is referred to as Gas Tungsten Arc Welding (GTAW) in USA and Wolfram Inert Gas Welding (WIGW) in Germany [Ahmad & Arya, 2018]. TIG welding is one of the oldest material joining process which was invented during world war-II [Waleed & Subbaiah, 2017]. This welding method is used to form high quality welds of a variety of materials such as aluminium, stainless steel, titanium etc. This process is best suited for joining thin sections. In TIG welding, an electric arc is formed between an inconsumable tungsten electrode and the workpiece (base metal). The arc provides the thermal energy to melt the workpieces as well as the filler if necessary [Munoz et al., 2017]. Non-consumable electrodes come in various sizes and lengths and are typically made of pure tungsten or an alloy of tungsten and other elements and oxides. The tungsten electrode is shielded by a gas nozzle in order to use shielding gas more effectively. 100% pure argon is the most preferred used shielding gas, to protect the weld pool from oxidation

and from nitrogen absorption, but sometimes helium is used too [Waleed & Subbaiah, 2017].

During the TIG welding heat is generated through the arc of electricity which moves from the tungsten electrode to the base metal surface to be welded. TIG welding utilizes a suitable power source, a welding torch having connections of cable for current, tubing for shielding gas supply, and tubing for water for cooling the torch. The electrode is mounted in a special electrode holder. This electrode holder is also designed to furnish a flow of inert gas around the electrode and around the arc. Welding operation is done by striking the arc between the workpiece and tungsten electrode in an atmosphere of inert gas. The arc is struck either by touching the electrode with a scrap metal tungsten piece or using a high-frequency unit. After striking the arc, it impinges on the workpieces forming a molten weld pool. The welding is started by moving the torch along the joint and is stopped at the other end by increasing the arc length. The shield gas is allowed to impinge on the solidifying weld pool for a few seconds even after the arc is extinguished. This will avoid atmospheric contamination of the weld metal. The welding torch and filler metal are generally kept inclined at angles of 70 degrees – 80 degrees and 10-20 degrees respectively with the flat workpiece [Ahmad & Arya, 2018].

1.1.2 Friction Stir Welding

Friction stir welding (FSW) is defined as a unique welding method and new invention for the welding technology world. FSW is recognized as a very attractive joining method for aluminium because of its many superior features, such as small degree of initial imperfections, low level of energy consumption and there are no harmful gas emissions [Paik, 2009]. FSW technology is mostly used in building various aluminium structures, such as railcars, automobiles and bridges. FSW process is said to be energy efficient, environmentally friendly and versatile. FSW is the most significant development in metal joining in almost three decades [Mishra and Ma, 2005].

The FSW technique works as follows: The work-pieces are clamped on the bed of the machine to avoid movements during welding. Work-pieces should be abutting meaning that both parts should be kept side to side at a particular distance from each other. Blunt or probe tool is then inserted. The shoulder gets in touch with the abutting edges. The rotating tool starts to be in contact with the pieces to be welded and create heat due to

friction. This heat makes the metal to melt plastically. When the metal gets plasticized the high downward forces or pressure keeps the plasticized material to form weld [Grill, 2017].

FSW is suitable to join high-strength aluminium alloys (7075, 6061,6063, 2024, 5052) and other metallic alloys that are difficult to weld by conventional fusion welding. The high strength and ductility of the material rely on the microstructural arrangement of that particular material. The fine and homogenous grain size yield better mechanical properties of a material. This then suggests that there should be a process which can be used to improve the material's mechanical properties post its production. Friction stir processing was found to be one of the mechanical techniques that could be used to improve the mechanical properties of the material [Mcnelley, 2011].

1.1.3 Friction Stir Processing

Friction stir processing (FSP) is a solid-state technique involving the use of a non-consumable rotating tool to refine and homogenize microstructures in metallic components or metals. It is among the allied processes of friction stir welding which were originally developed by The Welding Institute. Friction Stir Processing uses the same principle as friction stir welding (see figure 1), but does not join metals rather modifies the local microstructure in the near-surface layer of metals [Sun, 2009].

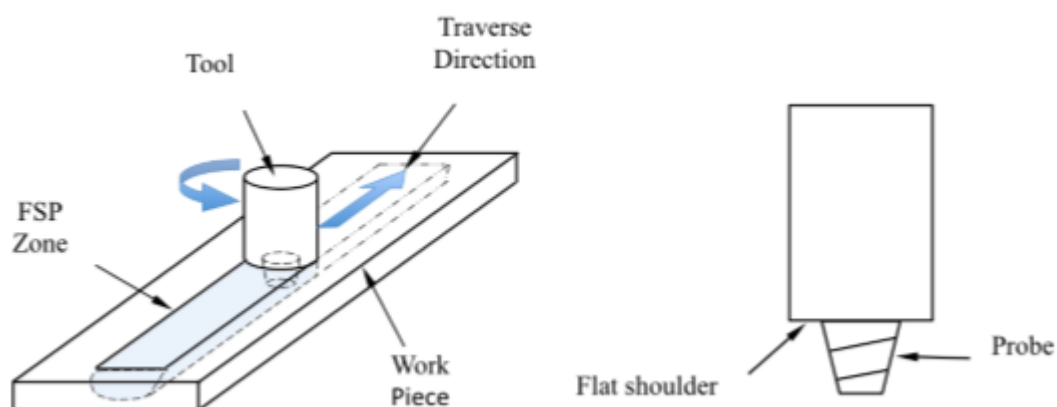


Figure 1: Schematic diagram of FSP setup and rotating tool [Sun, 2009].

To perform friction stir process to a certain location on a plate or sheet, a specially designed cylindrical tool is used. The rotating pin contacts the surface and rapidly friction

heats and softens a small column of metal. The tool shoulder and length of entry probe control the penetration depth. When the shoulder contacts the metal surface, its rotation creates additional frictional heat and plasticizes a larger cylindrical metal column around the inserted pin. The shoulder provides a forging force that contains the upward metal flow caused by the tool pin. During FSP, the area to be processed and the tool are moved relative to each other such that the tool traverses, with overlapping passes, until the entire selected area is completely processed [Kumar et al., 2012].

1.2 Problem Statement

Materials processing is as old as civilization. England started machine automation for forming, shaping and cutting in 18th to the 19th century. Since then, materials-processing methods, techniques, and machinery have grown tremendously. Selection of material with specific properties is the key parameter in many industries, especially in the aircraft and automotive industries [Sun, 2009]. This study presents a comparative analysis between the mechanical properties of the friction stir processed TIG – welded joints and friction stir welded 5083 aluminium alloy joints.

1.3 Research Background

The concept of FSP is considered as being moderately new which then suggest that there are many areas which need a thorough investigation to optimize the process and make it commercially practical. As it was mentioned in the introduction that FSP is mostly used to improve the mechanical properties of the material. This suggests the alteration of the microstructure i.e. the refinement of the grain size and rearrangement of the grains. In order to obtain the finer grain size and rearrangement of grains in a material, certain process parameters like rotational and translation speeds, tool geometry etc., are to be controlled [Darras, 2005]. Several investigations are being carried out in order to study the effects of these process parameters on the grain structure and mechanical properties.

FSP is the latest microstructure modification technique and was derived from FSW which was invented by The Welding Institute (TWI) of the United Kingdom in 1991 [Grill, 2017]. FSP has recently become an efficient tool of homogenizing and refining of the grain structure of the metal. Therefore, it has great potential in the field of superplasticity.

Freeney (2007) did a study on the feasibility and benefits of using friction stir processing as a thermo-mechanical microstructural modification tool for enhancement of magnesium alloys, specifically high strength EV31A and WE43. The employment of FSP resulted in the grain size reduction on EV31A. It was further discovered that FSP brought about the breakage and dissolution of second phase particles. The results showed significant strength and ductility improvements post FSP. FSP was also found to be a good technique in refining the microstructure of AM60 magnesium alloy [Iwaszko et al., 2016]. There was a notable improvement on the microstructure of the processed magnesium alloy compared to the unprocessed one. The FSP technique also brought an elongated and deformed grain distributions along the TMAZ region. These grains were also found to be homogenous compared to the unprocessed magnesium.

Saini et al. (2015) modified the surface of cast Al-17%Si alloys using friction stir processing. The aim of this modification was to evaluate the effect of input process parameters of friction stir processing to enhance the mechanical and tribological performance of the cast hypereutectic Al-17%Si alloy. It was discovered that the microstructure of cast alloy was improved and the Si was uniformly distributed. The reduction in porosity was prominent. The hardness and tensile properties were improved compared to the raw material. The tensile elongation was increased from < 2 % to about 9 %. The impact of processing the 6mm thick aluminium AA7075 – T651 was studied by Murthy and Rajaprakash (2018). This study focused more on evaluating the tribological and mechanical properties of this material. The results showed that the hardness, wear rate of the friction stir processed was enhanced by 44% and 60% respectively compared to that of the unprocessed material.

Based on the previous work, it is apparently clear that FSP could be employed to enhance the properties of a single piece of material. There is no trace of the previous work where the FSP is used as the post-processing on welded joints. This work is looking at analysing the processed TIG and FSW welded joints.

1.4 Research Objectives

The objectives of the research are as follows:

- To characterise the mechanical properties of friction stir processed TIG welded and friction stir welded 5083 aluminium plate.

- To compare the processed joints with some unprocessed ones

1.5 Review of Related Literature

This section gives a summarized version of work previously performed on FSP to improve mechanical properties of the material. The first work on FSP was reported by Mishra et al. (1999) where they used FSP in enhancing the strain rate plasticity of 7075 aluminium alloy. Since then, FSP was employed to perform various modifications and this includes the fabrication of surface composite.

Mcnelley (2011) investigated the refining of microstructure and improvement of mechanical properties of the continuously cast AA5083. The process parameters used were a tool rotation speed of 800rpm, a traverse speed of 76.2mm/min and a step-over distance of 2mm. The results showed grain reduction from 70 μ m in the base metal to 4 μ m in the friction stir processed zone. Furthermore, the results showed improved ductility of the FSP material which correlated to grain refinement and microstructure homogenization.

The processing of cast aluminium A206 plate reduced the size of the grains compared to the unprocessed regions of the plate. The microhardness was increased compared to the unprocessed regions. The processing of this material was also found to have contributed towards the improvement of its tensile strength [Sun, 2012]. There are different types of parameters that are involved in FSP. This includes welding speeds, rotational speeds, etc. The good combination of these parameters suggests the achievement of a good product. SSM 356 aluminium alloy was used to study the impact of welding and rotational speeds towards the mechanical properties of this material [Chainarong et al., 2014]. These speeds were varied with the purpose of obtaining the optimum combination. The rotational and travelling speeds of 1750 rpm and 160mm/min were found to be optimal values in obtaining an improved result. The results from this study showed a notable increase in microhardness and tensile strength of the processed region compared to the unprocessed one. The microstructural analysis also showed homogeneity on the processed region compared to the unprocessed one.

Sanusi and Akinlabi (2017) did a study on the employment of FSP technique in developing surface composites of aluminium alloy (AA 1050) reinforced with titanium

carbide (TiC) powder. The process parameters used were the rotational speeds of 1200rpm and 1600rpm and the travel rates of (100, 200 and 300) mm/min. The tests conducted in this work were the characterization of the microstructure, microhardness profiling and wear resistance tests. The results obtained from their study revealed that the microhardness profiling of the processed samples increased the hardness value compared to the parent material. The wear-resistance test results confirmed that the FSP technique enhanced properties in the surface region.

Based on relative literature, FSP has successfully refined the microstructure at the processed area which resulted in improved mechanical properties of different aluminium alloys. This therefore means FSP is one of the best processing technique for aluminium alloys. In this study FSP will be taken to task as a post-processing technique for TIG and FSW weld joints, analysing its impact on the respective mechanical properties.

1.6 Dissertation Outline

Chapter one presents the introduction, background, research objectives and the review of relative literature of FSP. Chapter two presents the detailed literature relative to the study and a summary about the reviewed literature. Chapter three presents the details about experimental setup and performances. Chapter four presents the results and discussions. Chapter five presents the conclusions for the study based on the results obtained.

CHAPTER TWO

LITERATURE REVIEW

This chapter presents a detailed literature review related to our research. The main focus is based on three subtopics which are the core of this study i.e. FSW, TIG and FSP.

2.1. Friction Stir Welding

The mechanical properties of friction stir welded joints of a 5 mm thick 1050 – H24 aluminium alloy were studied by Liu et al. (2013). The process parameters used included a tool tilt of 3°, tool rotation of 1500rpm and travelling speed ranging from 100 till 800mm/min. The tensile tests were executed for the evaluation of the mechanical properties of the FSW joints. The maximum tensile strength of the joints was found to be equivalent to 80% (178.68MPa) of that of the base material which was 100MPa.

The literature revealed the friction stir welding of similar aluminium alloys (6061 to 6061) using a 4mm thick plate [Rao and Rao, 2017]. Variable process parameters were employed to analyse the influence of microstructural and tensile properties. All welds were found to be defect free. FSW results showed an increase in the ultimate tensile strength and yield strength from 120MPa, and 55MPa to 240.78MPa and 215.54MPa respectively. Tensile strength and ductility showed more improvement when compared to the base material. FSW resulted in the Vickers microhardness (HV) of 370.

Aluminium alloy 2021-T4 sheets were friction stir welded by Yue et al., (2018). A 15mm diameter shoulder tool was used in the study to guarantee sufficient heat input during FSW. The root and tip diameters of the pin were 6mm and 5mm respectively. The length of the pin was 0.6mm. The results showed hardness of the stir zone showed a decrease of about 6% compared with that of the base metal. A maximum tensile strength of 399.5MPa and an elongation of 5.6% were achieved at 1000 rpm and 150 mm/min. The obtained UTS results showed an increase of 9.45% in comparison to the AA2021-T4 base metal. The SEM results showed the fracture morphology of a typical ductile fracture mode.

The microstructure and mechanical properties of friction stir welded AZ61 magnesium alloy joint was studied by Singh et al. (2018). A 4mm thick with 150mm length and 50mm width AZ61 magnesium alloy plate was utilised. The tool with a shoulder diameter of 18mm, the pin diameter of 6mm and the pin length of 3.8mm was used. The constant rotational speed of 1400rpm and a travelling speed of 25mm/min were utilized in this study. The tests performed on the joints were welding defects, microstructure, microhardness and tensile tests. The UTS of 220MPa, the yield strength of 175MPa and the elongation of 7.2% were obtained from the results. The weld joint UTS had a decrease of 29.03% while yield stress showed an increase of 34.62% in comparison with the parent material. Elongation also showed a decrease of 55% in comparison with that of the parent material. The dimples observed on the fractured surfaces indicated that the joint failed in a ductile mode.

2.2 FSW of Aluminium Alloys

The FSW welded joint of AA6351 aluminium alloy was recently analysed in comparison to the parent material [Palanivel et al., 2011]. The AA6351 plates with dimensions of 100mm long, 50mm wide and 6mm thick were used. The controlled parameters used for this study were welding speed of 2.5mm/min, rotating speed of 1500rpm and an axial force of 2kN. The tensile tests were conducted. The decrease in some values of FSW results was noted. The UTS, yield strength and percentage elongation were lower when compared to those of the base material.

A similar study was also performed on the 6061-T6 aluminium alloy [Chandu et al., 2014]. A 6mm thick, 150mm length, 70mm width AA6061-T6 was used. The welding parameters used were the tool rotation of 1200rpm, the axial force of 7kN and welding speed of 28mm/min. The tensile tests and Brinell hardness tests were conducted. The FSW results showed increased maximum yield strength, UTS and percentage elongation. The hardness had a notable increase of 76.3% compared to the base material.

The AA5086 plates were friction stir welded with the aim to analyse the microstructural characterization, mechanical properties and corrosion resistance [Chen, 2014]. The AA5086 plates were friction stir welded vertically to the rolling direction with a travel speed of 20mm/min and a rotational speed of 1000rpm. The tests conducted included the tensile tests, microhardness tests and microstructural tests. The tensile results obtained were the elongation of 16.7%, UTS of 300MPa and yield strength of 237MPa.

As compared to the BM, FSW had lower tensile and yield strength values, which attributed to the weld zone having a lower hardness than the BM. However, the ductility of the two FSW specimens increased as compared to that of the BM. The FSW tensile results were found to be inversely proportional to those of the hardness (HV) which showed a decrease compared to base material ones. The fracture surfaces of tensile specimens were characterised using SEM. The fractographs showed dimpled fracture patterns of a typical ductile morphology. The tensile results correlated with the microstructural results giving refinement in grain sizes of the FSW weld joint when compared to the base material one.

The investigation on the mechanical properties on friction stir welding of a 4mm thick AA5052 was conducted by Nur et al. (2017). The welding parameters used for FSW included 50mm/min welding speed, 1300rpm rotating speed for the first batch. Process parameters for the second batch were 208mm/min and 855rpm for welding speed and rotating speed respectively. The mechanical properties analysed included tensile strength and flexural strength. The ultimate tensile strength was found to be 222.1MPa and 213.4MPa for first and second batches of the specimen. The obtained friction stir welded AA5052 UTS results for both batches were lower than that of the base material.

It was demonstrated that the milling machine can be reconfigured such that it performs FSW [Sarma, 2018]. In-house design and manufacturing of the tools were performed using steel. The optimum parameters of 1000rpm and 80mm/min for rotating speed and traverse speed were selected for the performance of welding. The mechanical properties of the joints were analysed by the performance of tests and hardness tests. The results showed an increased hardness for the welded joints in comparison with base metal hardness. The UTS for the FSW specimen was 66.89MPa which was far lower than that of the base metal (310MPa). This decrease in the UTS was assumed to be caused by the vibration of the tool due to its eccentricity. Furthermore, there was an inverse relationship between the UTS and hardness of the welded joints.

2.3 TIG Welding of Aluminium alloys

Narayanan et al. (2013) TIG welded the aluminium alloy 5083. The welding parameters used were the welding currents of 200A and shielding gas flow rate of 15 l/min. Various tests like a tensile test; microhardness, macrostructure and microstructure study were conducted on the welded specimens. The test results showed the ultimate tensile

strength of 281MPa, the hardness of weld metal of 73.5HVN. The obtained results were lower in comparison with the commercial mechanical properties of the AA5083 in which the UTS is 317MPa and hardness is 96HVN. In the heat affected zone precipitates were formed resulting in less elongation and increase in hardness, so the brittleness of material increased and the tensile strength of material decreased when compared to the base material.

A study on improving the welding quality of AA6031 plates using an automated TIG welding system was performed by Mohan (2014). The welding parameters used were current of 180A, 50V voltage, welding speed ranged from 3.5-5mm/s, and a gas flow rate of 8-10l/min. The results showed a maximum tensile strength of 111.9MPa which was much lower than the tensile strength of the pure aluminium (90MPa). Additionally, the tensile strength of the weld joint seems to be depending on some welding parameters (welding speed and welding current). The tensile strength value of the welded joint decreased from about 110MPa to 75MPa as the welding speed increased from 3.5mm/s to 5mm/s. The hardness value of the weld zone change with the distance from weld centre due to change of the microstructure. For both sides, the welding tensile strength was found almost equivalent to the strength of base material.

The 12mm thick 5083 aluminium alloy was successfully TIG welded for the examination of the microstructure and mechanical properties on the welded joint [Xuebao, 2014]. A 12mm thick AA5083 plate and an ER536 filler wire were used. The results of the welded joint showed a fine and homogeneous microstructure in comparison to the base metal. The microstructure in the HAZ was slightly coarsened compared to the microstructure in the weld. The tensile strength of welded joints was over 90% of that of 5083 base metal. The welded joint had high strength and ductility when compared to the base material ones.

Singh et al. (2015) reported the mechanical properties of TIG welding at different parameters with and without the use of flux. The welding parameters used in the study included the welding current range of 105-140A, arc voltage of 16–18V, electrode diameter of 1.6–2.4mm and the gas flow rate of 8–10l/min. The results showed that the hardness (HRC) decreased from 65 to 60.2 (without flux), and from 58 to 52.5 (with flux) when the current increased from 105 to 140A. The results also showed that the increase in diameter of an electrode resulted in an increase in the hardness value. Additionally,

the hardness of the weld joint was less in the case of welding without flux as compare to welding with flux.

The literature also reveals that the AA7005 aluminium alloy plate could be welded through the use of TIG welding technique [Patil and Shelke, 2016]. The parts to be joined in the study were arranged such that a V-groove butt joint was formed. The welding parameters used were the argon shielding gas, electrode diameter 3/32", root gap of 0mm, filler material of AA5356, filler material diameter ranging from 1.5 to 2.4mm and welding voltage ranging between 50 and 100V. Oxide flux powder SiO₂ was used along with acetone. The results showed the tensile strength increased from 347MPa to 356MPa with the increase in welding parameters (welding current, welding speed and gas flow rate). The results also showed that the hardness (BHN) increased (from 92 to 98) with the welding parameters. The results of the UTS and Hardness showed a great increase when compared to the base material ones.

Kumar-Singh et al. (2018) analysed the mechanical properties and microstructure of the AA5083 on the TIG welded joints. A constant current of 134A and gas flow rate of 7l/min were used during welding. The results revealed that tensile strength increased with the increase in welding speed but this linear relationship was noted until the speed of 100mm/min. Subsequently, after 100mm/min, the tensile strength started to decrease as the welding speed continued to increase. The welding speed, current and gas flow rate were found to be very important parameters which were directly affecting the tensile strength of welded specimen and also plays an important role in metallurgical changes. The microstructure of the weld pool showed a refined grain size in comparison to the base metal.

2.4 FSP of Aluminium Alloys

The microstructural and mechanical characterization of the AA5086 through the use of FSP was reported in the literature [Pradeep et al., 2012]. The processing was carried out at a constant rotation speed of 1025rpm and at a traverse speed of 30mm/min. The tests conducted include microstructure tests, tensile tests and hardness tests (HV). The results showed an increase in the UTS and hardness of the processed single pass and multipass plates compared to those of the base material. The observed increase correlated with the microstructural grain size refinement in the nugget zone.

The effect of FSP on the mechanical properties of friction stir welded 7075 aluminium alloys plates was discovered by Resan et al. (2014). The process key parameters used were the rotating speed of 1700rpm and traverse speed of 40mm/min. The results showed that FSP increased the ultimate tensile strength from 390MPa to 434MPa and this is equivalent to a 9.3% improvement. There was about 5.2% notable increase in FSP hardness results compared to FSW. Furthermore, FSP produced refined microstructure grain sizes in comparison with FSW.

The 7039 aluminium alloy was friction stir processed for the analysis of mechanical properties in comparison to the base material ones [Sinhmar et al., 2015]. The modified surfaces were characterized in respect to macrostructure, microstructure, hardness and tensile properties. The results showed an increase in ductility from about 13.5% to 23.6% while the ultimate and yield strength were adversely affected. The results showed higher ductility on the longitudinal direction than in traverse direction. The multi-pass friction stir processing produced higher hardness than the single pass one. The friction stir processed AA7039 hardness test results were found to be lower than that of the unprocessed alloy.

Jweeg et al. (2015) did a comparative study on the mechanical properties of a friction stir processed aluminium alloy 5086-H32 in comparison to friction stir welded joint ones. The process parameters used for both FSP and FSW were rotational speed which consisted of three different rotational speed (750, 1000 and 1250) rpm and a traverse speed of 40mm/min. Tensile tests, bending tests, microhardness, microstructure tests were performed to analyse the mechanical properties. There was an observed increase in UTS results for the processed joint compared to the unprocessed one. The FSW joints showed lower bending force compared to that of FSP. Additionally, the microstructural grain sizes of FSP welded joints were slightly finer than FSW joints. The hardness (HV) of the FSP joints was higher than that of FSW joints. There was a correlation between the hardness and microstructural results of the FSP joints, as the hardness increased the microstructure grain sizes were refined.

The effect of FSP on AA2024-T3 was studied by Fadhel et al. (2015). A 5mm thick, 250mm long and 100mm wide plate was used. A vertical milling machine was used for the friction stir processing of the plate. The process parameters used included the flat

pinless cylindrical shoulder of 10mm, rotational speed of 945rpm and a traverse speed of 85mm/min. Tensile test, microstructure analysis and hardness test were conducted. FSP resulted in an increase of hardness compared to the base material. An increase in the yield strength, percentage elongation and UTS compared to those of the base material was noted. The microstructure grain size refinement correlated with the tensile and hardness test results.

The rotating speed of 1300rpm and traverse speed of 60mm/min were used for the friction stir processing of 6061-T6 aluminium alloy [Salman et al., 2016]. The same parameters were used for FSW of the same alloy. The mechanical properties of FSP were studied comparatively with the FSW ones. The results showed a notable increase in UTS of the processed FSW compared to the unprocessed one. The increase in the tensile properties correlated with the microstructural grain size refinement of the processed alloy.

The investigation on the microstructure and tensile properties of friction stir processed Al-Si alloy was performed by Abdulmalik et al. (2018). A 5mm thick plate and a conical pin with an overlap of 50% were utilised. The main processing parameters used included fixed tool rotation speed of 1400rpm, traverse speed of 42mm/min and a tool angle of 3°. The results showed a high increase in percentage elongation of the processed plate in comparison to that of the base material. There was a notable increase present in the UTS of the processed plate compare to the BM correlating the refinement in the FSP grain size.

The microstructural modification of AA206 through the use of FSP was also reported in the literature [Sun et al., 2018]. This modification was performed so as to comparatively evaluate the mechanical properties of processed and unprocessed AA206 material. A 6.26mm and 16mm thick plates were used for tensile and fatigue test respectively. The two key processing parameters were tool rotation speed of 1000rpm and tool traverse speed of 50.8mm/min. The results showed an increase in both yield strength and UTS after FSP when compared to those of the base metal. There was a notable improvement in yield strength and UTS on the processed plates compared to the base material. The percentage of elongation and fatigue strength also increased compared to the unprocessed ones. The increase in these properties correlates with the grain size refinement and homogeneity.

AA6061-T6 plate was friction stir processed using various process parameters [Gopan et al., 2018]. The key parameters used included tool rotational speed of 500rpm, transverse feed of 14mm/min and plunge depth of 3.1mm. It was observed that the increase in rotational speed led to a decrease in hardness value. There was a notable increase in the hardness value of the processed AA6061-T6 compared to the unprocessed ones.

The effect of friction stir processing welding parameters on the microstructure and mechanical properties of A384 aluminium alloy was successfully evaluated [Abdel-Aziz et al., 2018]. Water was used as a cooling medium during the process in the study. The results revealed higher values of tensile properties at the rotational speed of 1200 rpm and travel speed of 80 mm/min. There was an improvement in the processed UTS and YS in comparison to the base material ones. The microstructure results revealed that FSP refined the grain sizes which contributed to the and improvement of ductility.

2.5 Summary

In all the work that has been performed thus far, it has been noted that all the focus has been on FSP as an enhancement technique on aluminium alloys, magnesium and other alloys. It is also noticed that the common mechanical properties analysed include the tensile test, fatigue and microhardness. These properties are studied correlatively with the microstructure. The 6mm thickness seems to be the most used thickness towards the performance of either FSW or FSP. Little to no work reported which has considered FSP as a post weld processing technique for TIG joint. The focus of this study was based on using FSP as a post-processing technique to the weld joints of TIG and FSW. The mechanical properties of the processed joints are studied comparatively with the unprocessed ones.

CHAPTER THREE

EXPERIMENTAL SETUP AND PERFORMANCE

This chapter discusses the equipment used in performing all the experiments related to our study. This includes the welding techniques used in producing the welds that were friction stir processed. There are two welding techniques (FSW and TIG) employed in producing the required welds for our experiments. The welding conditions are being explained in this chapter. The details about the tests that were performed to the processed welds are also given with details in this chapter.

3.1 Welding Setup

The following are the equipment used in producing the welds:

- Guillotine Shear master cutting machine
- TIG machine
- Friction stir welding machine

3.1.1 Guillotine Shear Master Cutting Machine

The guillotine shear master machine illustrated in figure 3.1.1 is a multipurpose machine used in the cutting of alloys and other sheet metals into desired dimensions. The first step before using the shear master is to mark the plates or sheets to be cut for easy alignment. The plates get aligned with the shear master blade using the markings, then the cutting blade is lowered by pressing the foot pedal to execute the cutting. The cut off piece falls off to the box provided.

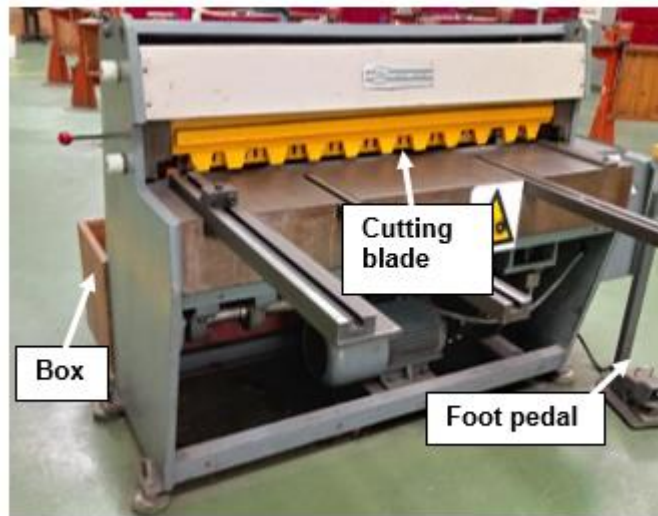


Figure 3.1.1: Guillotine shear master cutting machine.

3.1.2 TIG Welding Equipment

Figure 3.1.2 shows the TIG welding machine. The machine and its operating procedure were defined and explained in chapter one section 1.1.1.



Figure 3.1.2: TIG welding machine.

3.1.3 Friction Stir Welding Machine

The friction stir welding machine was successfully achieved from converting a conventional milling machine (see figure 3.1.3). More emphasis on FSW has already been given in chapter one, section 1.1.2. The same machine can also be used for friction stir processing technique.

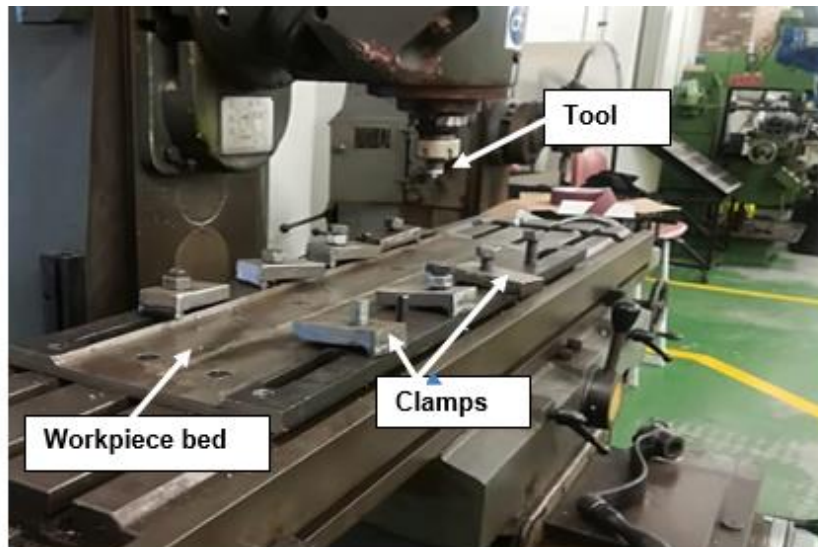


Figure 3.1.3: FSW machine.

3.2 Welding Performance

The plates were welded using the two previously mentioned techniques i.e. friction stir welding and TIG welding techniques. Prior to welding, the plates were cut into dimensions suitable for the FSW bed since the friction stir processing was performed using the FSW machine. Guillotine machine was used to cut the 6mm thick aluminium plates into 70mm wide and 530mm long. Figure 3.2 shows the cut plates ready for welding.



Figure 3.2: Aluminium set of plates used.

3.2.1 TIG Process

It should be noted that the TIG welding was outsourced due to the technical problems experienced by our TIG welding machine. The TIG welded plate is shown in figure 3.2.1.



Figure 3.2.1: TIG welded plate.

3.2.2 Friction Stir Welding

Friction stir welding was performed on the two AA 5083 6mm thick plates. The plates were fixed to the FSW machine bed using bolt and clamps to avoid movements during the FSW process (see figure 3.2.2 (a)). FSW was successfully carried out using a tool, presented in 3.2.2(b). The tool was made of tool high carbon steel material and this tool was a fixed type of a tool, meaning that the probe was fixed and was suitable for this kind of study since the workpieces had a uniform thickness. The diameter of the tool shoulder was 20mm, and at the end of the shoulder was a tapered probe with the length of 5mm. The tilt angle used during welding was 3° .

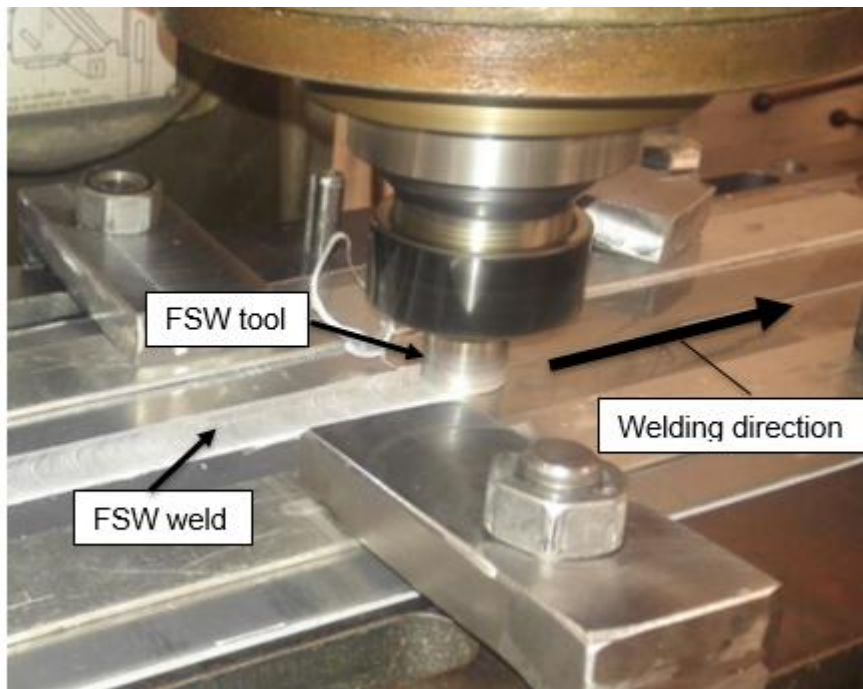


Figure 3.2.2: (a) FSW process.

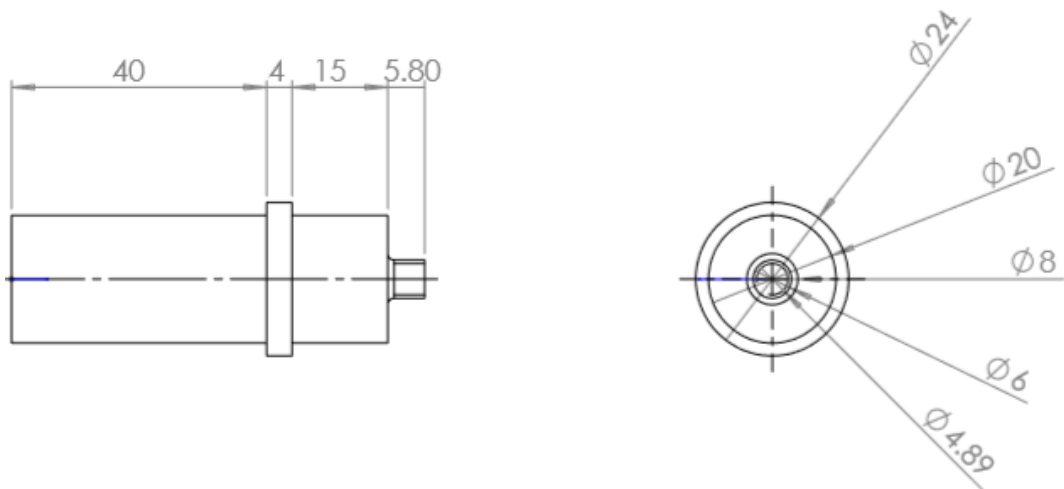


Figure 3.2.2: (b) Pin dimensions in mm.

Single pass welding procedure was used to fabricate the joints. No special treatment was carried out before welding. The welding parameters used for FSW are as presented in Table 3.2.2.

Table 3.2.2: FSW parameters.

Rotational Speed (rpm)	Welding speed (mm/min)	Vertical force (kN)	Traverse speed (mm/min)
1000	30	15	40

In performing the friction stir welding, the two aluminium alloy plates were clamped together tightly on the reconfigured milling machine bed. The welding speed, traverse speed and rotational speed were set. The rotating friction stir welding tool was plunged into the plates and kept stationary for a few seconds. This was done so as to allow the temperature to stabilize. The rotating tool was then released so that it travelled along both edges of the two plates that were welded. The rotating tool travelled from the start to the end of the plates resulting in the attainment of the weld. The tool was then unplunged, leaving a small hole as shown in figure 3.2.2(c).



Figure 3.2.2: (c) FSW plate.

3.2.3 Friction Stir Processing

Friction stir processing was performed on the friction stir welded joint and on the TIG welded joint using the reconfigured milling machine. The parameters used to perform FSP welding were the same parameters used to perform FSW (Table 3.2.2). The performance of the FSP on the FSW welded joints is depicted in figure 3.2.3(a). The processed FSW plate shown in figure 3.2.3(b) has two small holes towards the end. The holes were made by the tool as it was unplunging at the end of the FSW process and FSP process. Figure 3.2.3(c) depicts the FSP performance on the TIG welded joint. The processed TIG welded plate is shown in figure 3.2.3(d) with one FSP unplunged hole.



Figure 3.2.3: (a) FSP application on FSW welded joint.

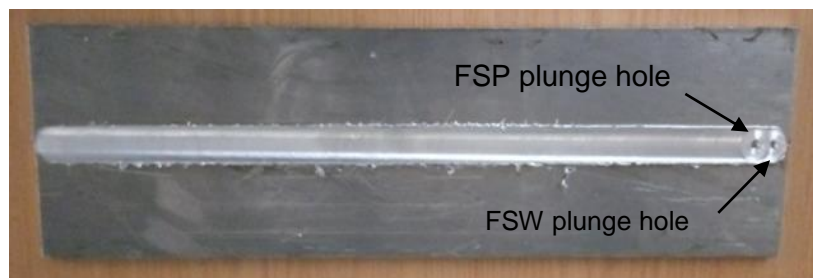


Figure 3.2.3: (b) Processed FSW plate.

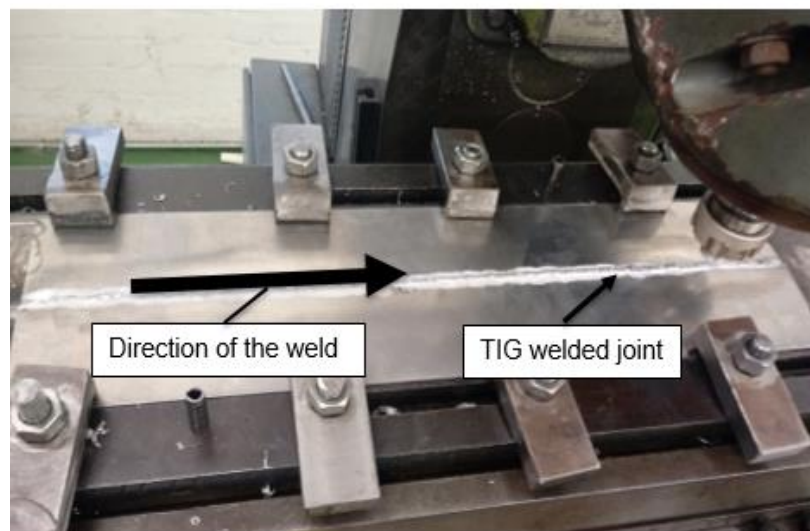


Figure 3.2.3: (c) FSP application on TIG plate setup.



Figure 3.2.3: (d) Processed TIG joint plate.

3.3 Weldments Analysis Preparation

The following are the list of equipment and techniques used in analysing the weld joints obtained through the steps explained under section 3.2:

- EDM Wire Cut Accutex AU-5001A Machine
- Struers Labopress-3 Mounting Press Machine
- Struers LaboPol-5 polishing machine

3.3.1 EDM Wire Cut Accutex AU-5001A Machine

Wire cutting is a cutting process whereby a thin single brass strand wire is fed through the workpiece that is submerged under water. The EDM wire cutting (see figure 3.3.1) exerts no cutting force on the workpiece and introduces no residual stress [Rogers, 2018]. Another advantage of wire cutting is that it has the finest surface finish, no additional polishing or finishing needed. The EDM wire cutting machining works by creating an electrical discharge between the wire and the workpiece. As the spark jumps across the gap, the material is then removed from the workpiece and the electrode. Due to the inherent properties of the process, the machine can easily machine complex parts and precision components out of hard conductive materials.



Figure 3.3.1: Wire cut machine.

3.3.2 Struers Labopress-3 Mounting Press Machine

The Struers labopress-3 machine shown in figure 3.3.2 is a machine that is used for mounting specimen in a hard epoxy resin. The mounting machine works by placing the specimen on the ram. A suitable resin is then filled into the cylinder through the funnel. The mould release agent is applied to all accessible surfaces of the upper ram. The top closure is placed on the mounting cylinder and pressed down counter clockwise. The next step is to set the force, heating time, heating temperature and cooling time, the process runs automatically as the start button is pressed.



Figure 3.3.2: Mounting press machine.

3.3.3 Struers LaboPol-5 polishing machine

The Struers labopol-5 presented in figure 3.3.3 is a polishing machine that grinds and polishes any kind of metals. The machine works by mounting a selected grinding or polishing disc onto the machine, then the speed is set (ranging between 50 - 500 rpm). The start button is then pressed to start the polishing process until the desired surface finish is reached.



Figure 3.3.3: Polishing machine.

3.4 Performance of Specimen Preparation

This section covers the preparation of the specimens for all the tests conducted.

3.4.1 Tensile Tests Specimen Preparation

The ASTM E8 standard was used to design the specimen and its geometry. The specimen dimensions (in mm) are illustrated in figure 3.4.1(a). The dog bone shaped specimen was first drawn using the AutoCAD design software, then cut using the EDM wire cut accurateX AU-5001A machine. Sample of a completed tensile test specimen is presented in figure 3.4.1(b).

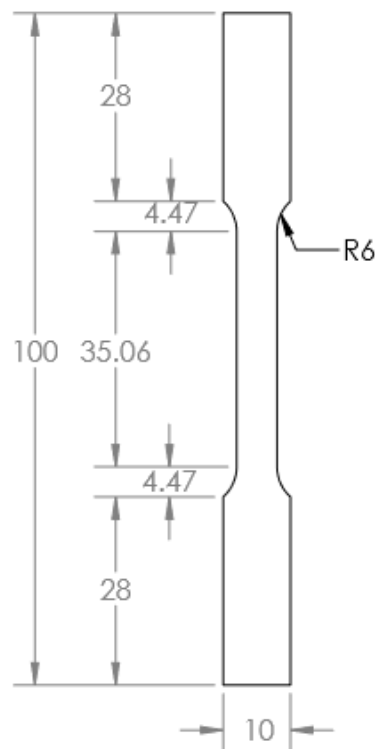


Figure 3.4.1: (a) Tensile test specimen with dimensions.



Figure 3.4.1: (b) Sample of a tensile test specimen.

3.4.2 Bending Tests Specimen Preparations

The standard followed to come up with the specimen design and geometry was the ASTM E290. The bending specimen dimensions were 20mm x 135mm x 6mm, (see figure 3.4.2(a)). The specimens were cut using the EDM wire cut accuteX AU-5001A machine. Finished sample of specimens is illustrated in figure 3.4.2(b).

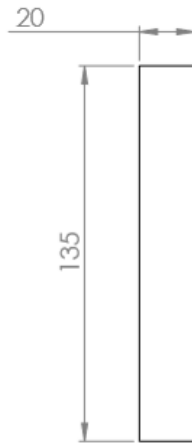


Figure 3.4.2: (a) Bending test specimen with dimension in mm.



Figure 3.4.2: (b) Sample of a bending specimen.

3.4.3 Microstructural Tests Specimen Preparation

The microstructure specimens shown in figure 3.4.3(a) were drawn and dimensioned using AutoCAD design software. The designed specimens were cut using the EDM wire cutting machine, see figure 3.4.3(b). The cut specimens were then mounted in thermosetting plastic using Struers labopress-3 machine and the mounting temperature was 150°C. The sample of the mounted specimen is shown in figure 3.4.3(c). The mounted specimens were then prepared for microstructural analysis. The preparation involved the use of Struers laboPol-5. Different sizes of sandpapers were used in order to obtain the final product shown in figure 3.4.3(d)].

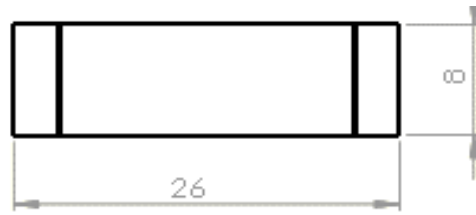
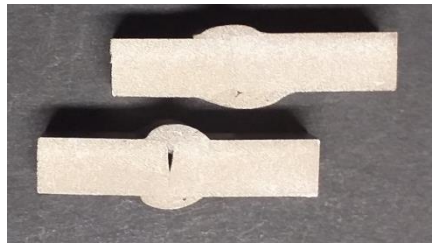


Figure 3.4.3: (a) Overall dimensioned microstructure test specimen.



3.4.3: (b) Wire cut microstructure specimen samples.



Figure 3.4.3: (c) Mounted microstructure test specimen sample.



Figure 3.4.3: (d) Polished specimen samples.

The polished specimens were immersed in 0.5% of hydrofluoric acid for 5 minutes. The specimen was then removed from the etchant and immediately rinsed with water and alcohol. The alcohol was dried off the specimen using a hot hair dryer. The fully prepared (etched) specimen is shown in figure 3.4.3(e).



Figure 3.4.3: (e) Etched specimen samples.

3.4.4 Hardness Tests Specimens

The specimens used for hardness testing had the same dimension as the ones used for microstructure testing, duplicates were made, one pair for hardness and one pair for microstructure. The same preparation performed for the microstructure test specimens was also performed for the hardness test specimens, the only difference was that the hardness test specimens were not etched, see figure 3.4.4.



Figure 3.4.4: Hardness test sample specimens.

3.5 List of Test Performed

It should be noted that the analysis was performed on the processed joints and unprocessed joints with the purpose of comparing the differences. The following is the list of tests that were performed:

- Bending Tests
- Tensile Tests
- Hardness Tests

- Microstructural Test
- SEM Test

3.6 Mechanical Tests

Different set of specimens were cut out from the unprocessed TIG and FSW plates, as well as on the processed TIG and FSW plates. The prepared specimens were for tensile tests, bending tests, hardness tests, as well as for microstructure. All the specimens were cut in three regions of the plate and those being the start, middle, and the end of the plate. A total of three specimens for each test were prepared.

3.6.1 Tensile Test

The uniaxial tensile testing was performed in order to analyse the ultimate tensile strength, yield strength, % elongation, fracture strain and Young's modulus for all the processed and unprocessed welded joints. The computer operated Hounsfield 25K type of tensile testing machine illustrated in figure 3.6.1(a) was used for tensile tests. The dog bone shaped specimens were used. The tensile test parameters used are presented in table 3.6.1. The ASTM E8 standard for tension testing of metallic materials was used in this study for tensile testing.

Table 3.6.1: Tensile test parameters.

Speed (mm/min)	Extension range (mm)	Load range (kN)	Load cell (kN)
1	0-10	0-10	50

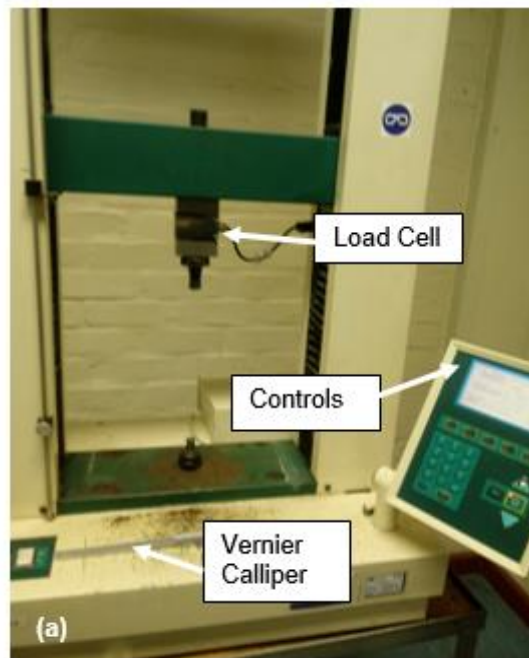


Figure 3.6.1: (a) Hounsfield machine.

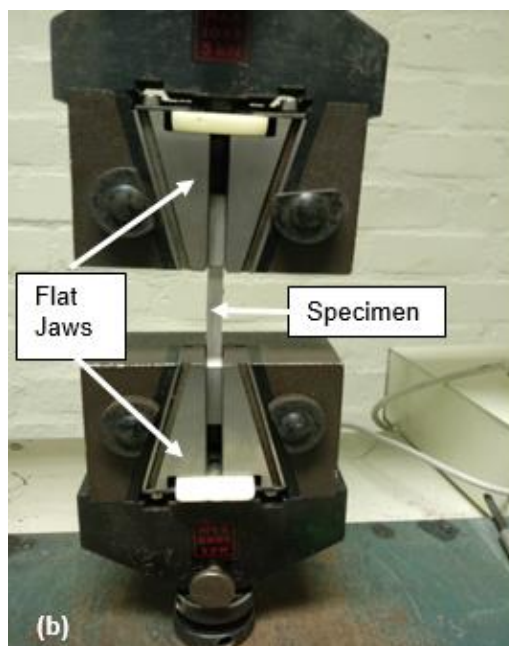


Figure 3.6.1: (b) Tensile testing flat jaws.

Prior to the installation of the specimens to the machine, the specimens' dimensions were measured and recorded, (thickness and gauge length), for the determination of the engineering stress and engineering strain. The specimen was fit into the jaws for gripping. The screws were tightened so as to avoid slipping during the test. The QMat software was used to log the data. The data logged was consisting of the applied tensile load and

extension which were later used for the determination of stress and strain. Young's modulus, yield strength, ultimate tensile strength, fracture strain, and percentage elongation were determined. The graph of stress versus strain was generated.

The following formula used to determine the ultimate tensile stress:

$$\sigma = \frac{F}{A} \quad (1)$$

Where σ is the ultimate tensile stress, F is the maximum force, A is the cross-sectional area.

The equation used to determine % elongation was:

$$\%E = \frac{\text{Final Length} - \text{Original Length}}{\text{original Length}} \times 100 \quad (2)$$

Elastic young's modulus was determined using the formula:

$$E = \frac{\sigma}{\delta} \quad (3)$$

where σ is stress and ϵ is a strain.

3.6.2 Bending Test

Bending testing is sometimes referred to as flex or flexural testing. This test was conducted to measure the flexural strength of all the AA5083 welded joints. Bending test was performed on the bending specimen using the Hounsfield testing machine with a 3-point bend fixture illustrated in figure 3.6.2(a). The bending test parameters were the same as the one used for tensile testing. The data was logged using the same procedure used for tensile testing.

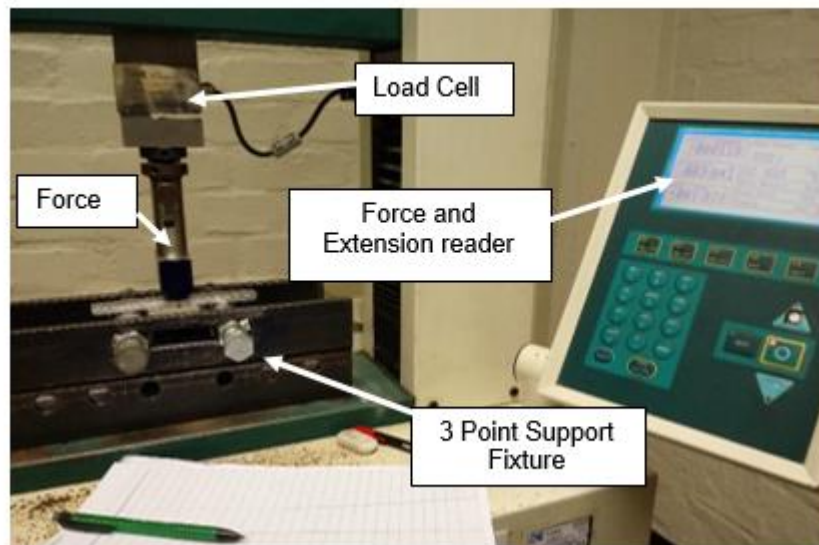


Figure 3.6.2: (a): Bending test setup and apparatus.

The first step in performing the bending test was to measure the specimen so as to verify dimensions. Center mark line was drawn on the centre of the joint for alignment with the centre of the indenter. The tests were performed one specimen at a time. The specimen was flat mounted on the rolling supports; the centre mark line was used to align the specimen with the loading pin centre. The loading pin was lowered until it was in contact with the specimen top surface. Thereafter the machine was zeroed before the commencement of the test. The force was recorded using 0.5mm extension increments. The data was logged from the beginning until the failure of the specimen.

The formulas used to determine the maximum stress was:

$$\sigma = \frac{3FL}{2bd^2} \quad (4)$$

where F is the force, b is the width of the specimen, L is the length, and d is the thickness, see figure 3.6.2(b) for schematic diagram for the bending test.

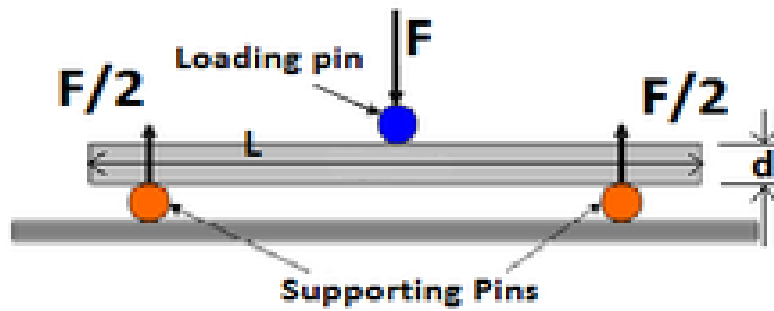


Figure 3.6.2: (b) Bending test schematic diagram [Ćurković, 2010].

3.6.3 Hardness Tester

The hardness test was performed to determine the bulk hardness of the AA5083 welded and processed joints. The test was performed using the Rockwell hardness testing FR model machine presented in figure 3.6.3. The apparatus used to perform the test were: ball indenter with a 1/16-inch diameter, Scale B (a scale for aluminium, copper, soft steel and malleable iron), a mass of 100kg.



Figure 3.6.3: Hardness test machine.

In performing the hardness testing, the specimen was placed on the machine flat stand. The stand was then adjusted upwards until the indenter came into contact with the specimen top surface. The reset button was pressed, then the autorun button was

pressed to start the process, and the Rockwell hardness number (HRB) was displayed and recorded.

3.6.4 Microstructural Tests

Microstructure analysis was performed to analyse the grain size of the weld joint. The microstructural analysis was performed on the prepared specimen using the Zeiss Axiovert 40 MAT optical microscopy shown in figure 3.6.4.

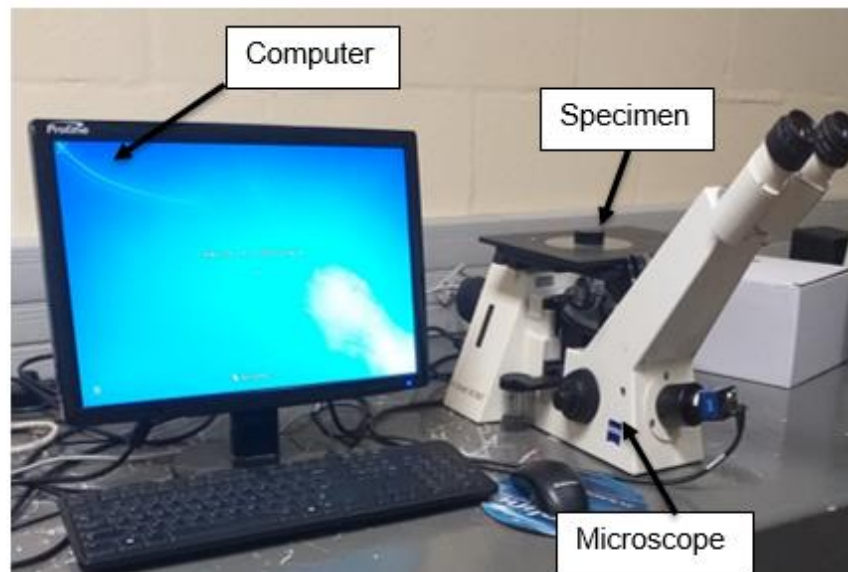


Figure 3.6.4: Microstructure apparatus.

In analysing the microstructure of the specimens, the etched specimen was placed onto the specimen bed with welding joints facing up for examination. The specimen was first examined at 5x magnification setting to observe larger features of the structure. Magnification of 100x was used to observe finer features. The grains were measured and recorded.

3.6.5 Scanning Electron Microscopy (SEM) Tests

SEM tests were performed using the post tensile test cut-off specimen. SEM tests were performed for identification of the nature of the fracture. The results for all the tests performed are presented in the next chapter.

CHAPTER FOUR

RESULTS AND DISCUSSIONS

This chapter gives detailed discussions on the results that were obtained through the processes and methods explained in chapter three. The results obtained include the bending test, the tensile test, hardness, microstructure and scanning electron microscopy results.

4.1 Bending Tests

This section presents the results that were obtained from the bending tests for three unprocessed FSW, processed FSW, unprocessed TIG and processed TIG specimens. It should be noted that there is a start location and ending location either in the processed plate or welded plate. So the three specimens were produced from the start, middle and the end of either welding or processing. This was performed so as to check if there were any notable impact on the results. The specimen that was cut at the beginning of the plate is marked with A, while B symbolizes the middle position and C is the end position of the plate. A, B and C represents unprocessed TIG and FSW specimens; A1, B1 and C1 represent processed TIG specimens and then A2, B2 and C2 represent processed FSW specimens. This representation was followed throughout the chapter. Figure 4.1 shows the demonstration of the specimen format for the processed FSW.

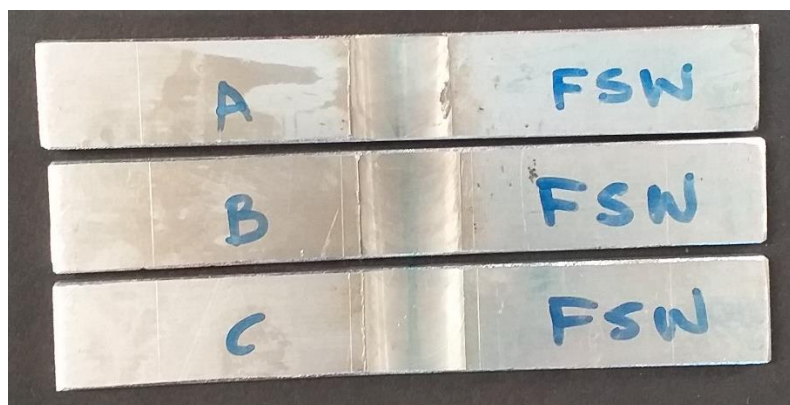


Figure 4.1: Sample specimen format.

4.1.1 Processed and Unprocessed TIG results

The bending was applied on both sides of the joint i.e. face and the root of each specimen. The face of the specimen is considered to be the surface that was in contact with the tool either during processing or welding. The root is the surface that was in contact with the welding or processing machine bed. Figure 4.1.1(a) shows the response of the unprocessed TIG welded specimens. The unprocessed TIG welded joints failed at the centre of the joint and the mode of failure shows that the plates were not bonded together but just the filler that dominated the joint. The root and face failure mode is exactly the same hence there was no need of including both results. The root and face failure modes are shown in figure 4.1.1(b) and (c). The opening of the crack for the unprocessed joint is higher compared to the processed one. This indicates the quality of bonding at the joint [Pradeep et al., 2012; Shalina et al., 2018].



Figure 4.1.1: (a) Bended TIG Specimen.



Figure 4.1.1: (b) Friction stir processed TIG (face) joints.



Figure 4.1.1: (c) Friction stir processed TIG, bended (root) specimens.

Figure 4.1.1(d) and figure 4.1.1(e) show the graphical representation of bending results for the processed and unprocessed TIG welded joint. It should be noted that all the specimens were bent until they fail hence the projectile-type of the graphs. For the face bending test, the unprocessed specimens failed at the maximum strain of 0.05 while the processed ones failed at the maximum strain of 0.25. For the root bending test, the unprocessed specimens failed at the maximum strain of 0.07 while the processed ones failed at the maximum strain of 0.29. The two graphs show a very clear distinction between the face bending test and the root bending test. The bending results also show that the processed joint is stronger than the unprocessed joint hence the difference in maximum strain. The graphical representation correlates with the failure mode shown by the pictures of specimens.

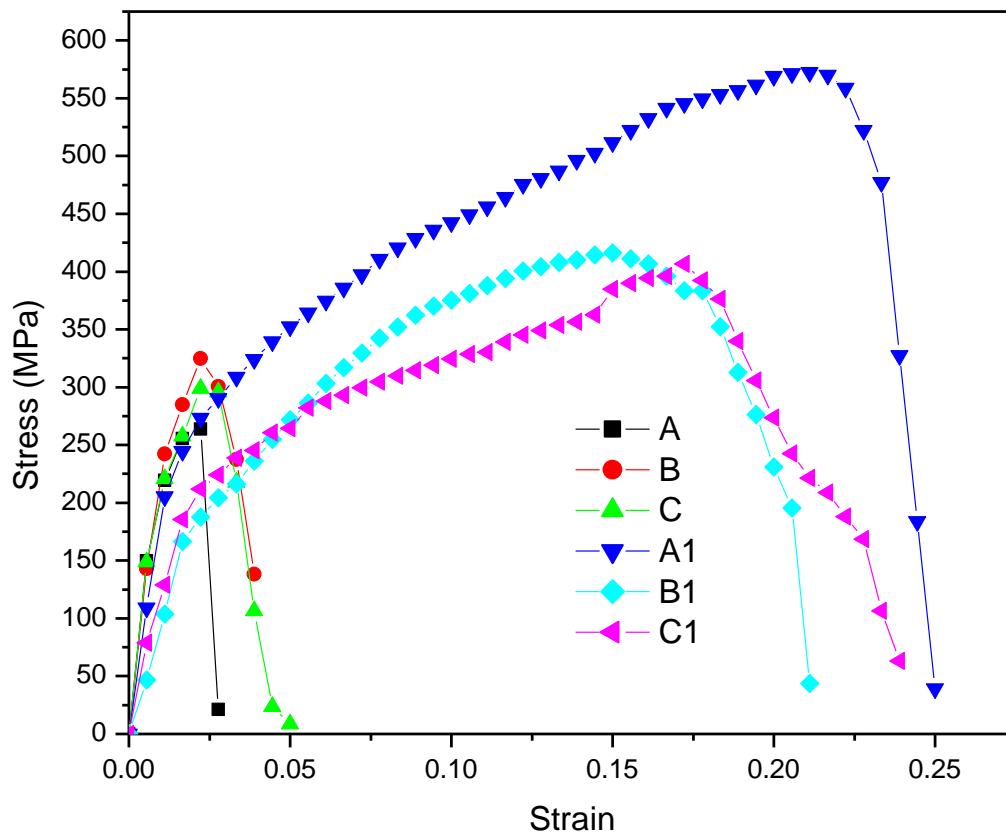


Figure 4.1.1: (d) Bending stress – strain curves for processed and unprocessed TIG (Face).

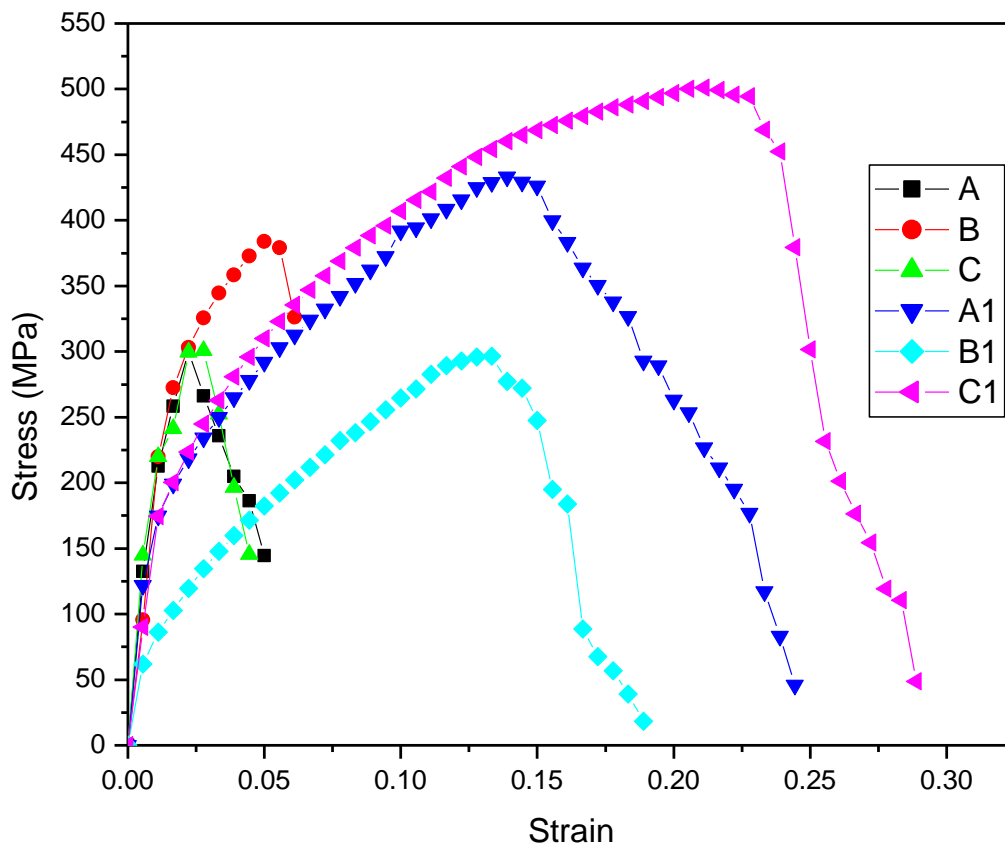


Figure 4.1.1: (e) Bending stress – strain curves for processed and unprocessed TIG (Root).

Table 4.1.1 shows the maximum deflection of each specimen tested. The processed TIG joint showed a maximum bending of 26mm while the unprocessed showed a maximum of 6mm on root bending specimen C1. The root bending results are higher compared to the face bending results. The maximum root flexural stress is 501.188 MPa while the maximum face flexural stress is 406.5 MPa. The notable consistent behaviour with the bending results is that the root bending is always higher than the face bending. The origin of this behaviour is not known yet but suspected to be caused by the surface finish of the two sides of the specimen.

Table 4.1.1: Processed and unprocessed TIG bending results.

Sample	Maximum Force	Fracture Point	Flexural Stress (MPa)	Post specimen
Face				
A	1407N, at 2mm	115N, at 3mm	263.813	Cracked
B	1733N, at 2mm	182N, at 4mm	324.938	Cracked
C	1593N, at 2mm	45N, at 4.5mm	298.688	Cracked
A1	3053N, at 19mm	210N, at 22.5mm	572.434	Cracked
B1	2193N, at 14mm	232N, at 19mm	416.063	Cracked
C1	2168N, at 15.5mm	337N, at 21.5mm	406.5	Cracked
Root				
A	1603N, at 2mm	69N, at 5mm	300.563	Cracked
B	2047N, at 4.5mm	90N, at 6mm	383.813	Cracked
C	1604N, at 2.5mm	45N, at 4.5mm	300.75	Cracked
A1	2310N, at 12.5mm	245N, at 22mm	425.063	Cracked
B1	1582N, at 12mm	98N, at 17mm	296.625	Cracked
C1	2673N, at 19mm	260N, at 26mm	501.188	Cracked

4.1.2 Processed and unprocessed FSW results

The type of bending performed under this section is similar to the one performed under section 4.1.1. Figure 4.1.2(a) and (b) show the face and the root failure mode for the unprocessed FSW. The face bent specimens show high crack intensity at the beginning of the plate compared to the end of the plate. The similar behaviour is also observed on the root bending results but the root results are much better than the face bending results. This crack variation is suspected to be caused by the instability of welding occurring at the beginning of the weld. The root bending results show the crack on the specimen cut at the beginning of the plate (specimen marked A) while the other two show no cracks at all. This indicates good bonding between the plates welded. The face and the root of the processed FSW are shown in figure 4.1.2(c) and (d). It is evident from the figure that the two surfaces bent without failing. This kind of behaviour suggests that the strength of the joint has improved.

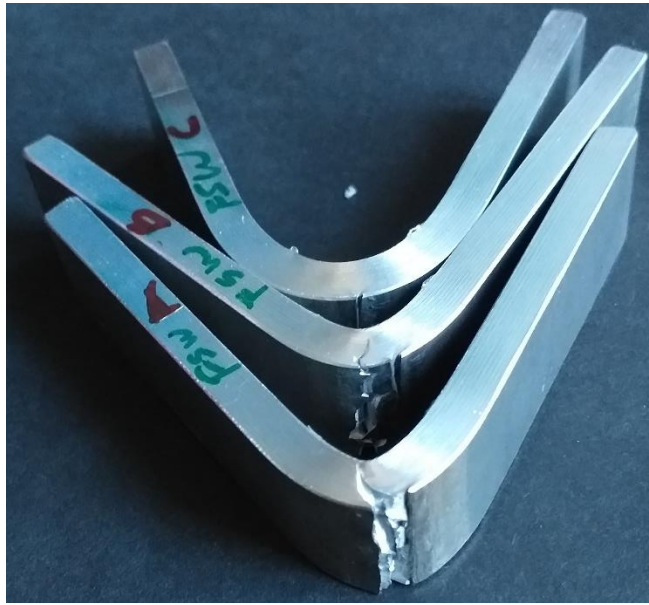


Figure 4.1.2: (a) FSW (Face), Bended specimens.



Figure 4.1.2: (b) FSW root bended specimens.



Figure 4.1.2: (c) Processed FSW (face), Bended specimens.



Figure 4.1.2: (d) Processed FSW (root) bended specimens.

Figure 4.1.2(e) and figure 4.1.2(f) show the graphical representation of bending results for the processed and unprocessed FSW welded joint. It should be noted that all the specimens were bent until they also fail. For the face bending test, the unprocessed specimens failed at the maximum strain of 0.325 while the processed ones failed at the maximum strain of 0.5525. The unprocessed root specimens failed at the maximum strain of 0.425 while the processed ones failed at the maximum strain of 0.60. The two graphs show a very clear distinction between the face bending test and the root bending test.

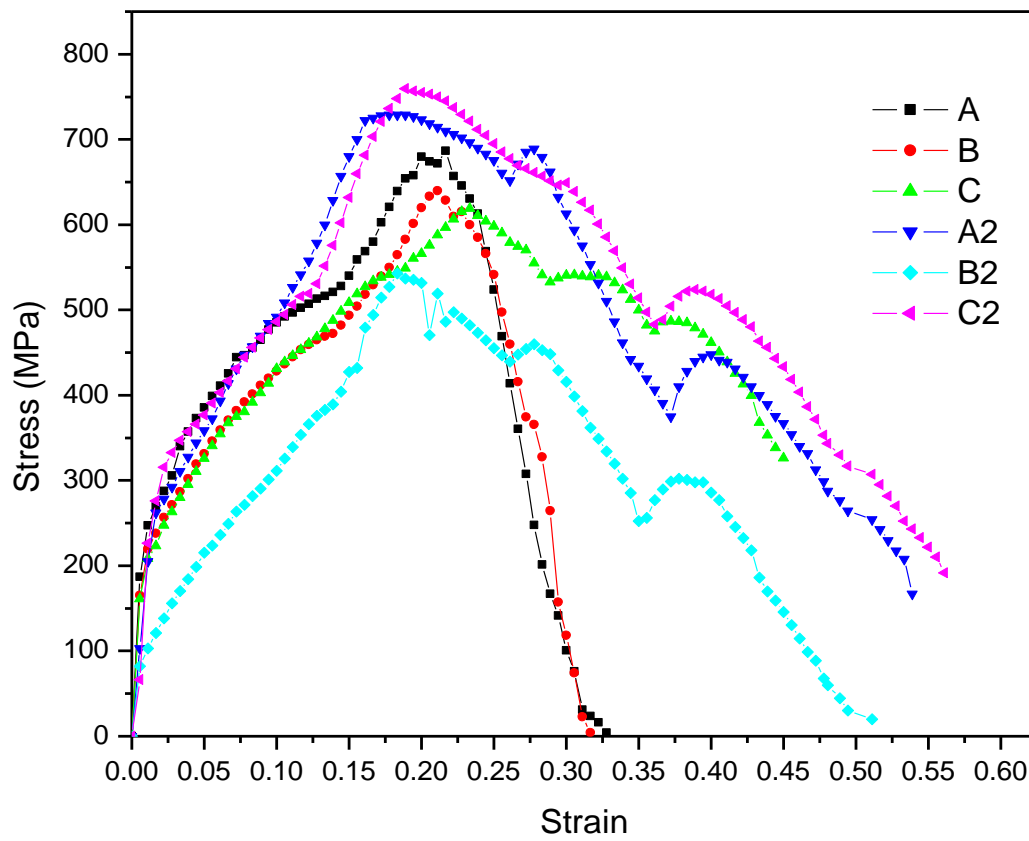


Figure 4.1.2: (e) Bending stress – strain curves for processed and unprocessed FSW (Face).

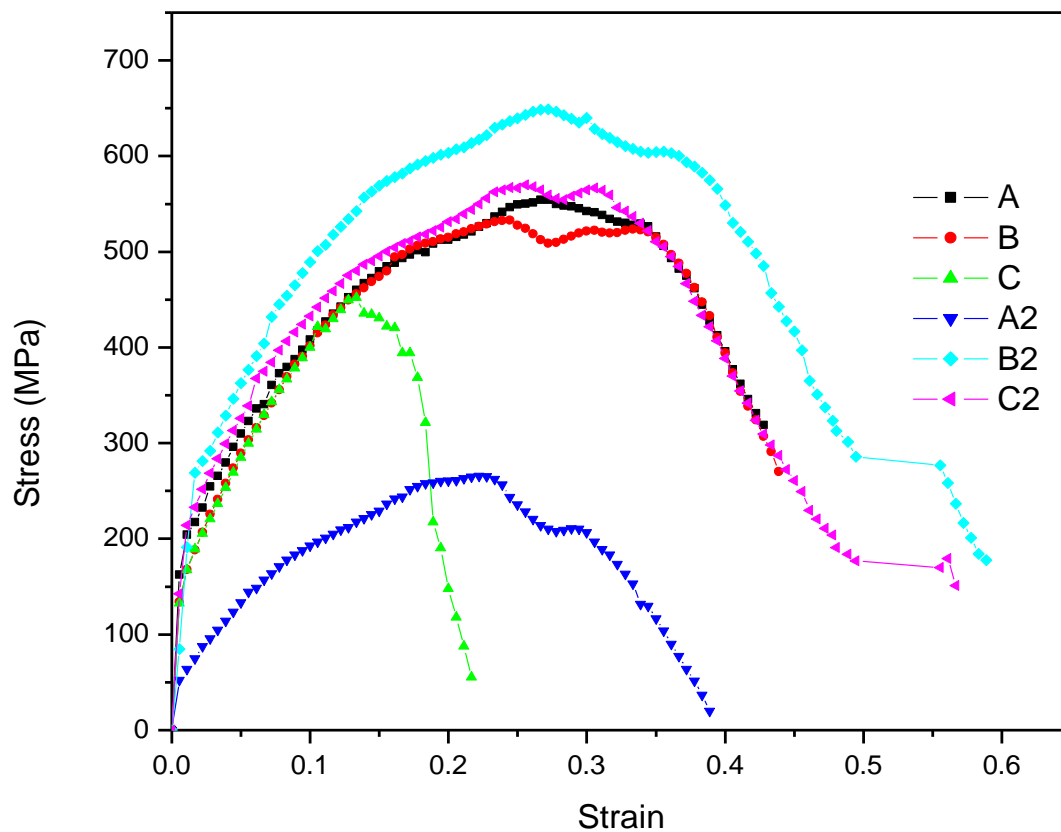


Figure 4.1.2: (f) Bending stress – strain curves for processed and unprocessed FSW (Root).

Table 4.1.2 shows the maximum deflection of each specimen tested. The processed face FSW joint showed a maximum bending of 49.5mm while the unprocessed showed a maximum of 40mm. The root bending results are lower compared to the face bending results. The maximum root flexural stress is 648.375 MPa while the maximum face flexural stress is 759.75 MPa. This behaviour is different from the behaviour that was noticed on the TIG joints analysis. It is noted that the processed FSW joint is more flexible compared to the processed TIG joint and this is judged from bending without cracks which also correspond to the flexural stress value.

Table 4.1.2: Unprocessed and processed FSW bending results.

Sample	Maximum Force	Fracture Point	Flexural Stress (MPa)	Post specimen
Face				
A	3662N, at 19.5mm	23N, at 29.5mm	686.625	Cracked
B	3412N, at 19mm	23N, at 28.5mm	639.75	Cracked
C	3301N, at 21mm	1740N, at 40.5mm	618.938	Cracked
A2	3888N, at 17mm	890N, at 47.5mm	536.625	No crack
B2	2895N, at 17mm	107N, at 45mm	759.75	No Crack
C2	4052N, at 17mm	1022N, at 49.5mm	729	No Crack
Root				
A	2957N, at 24mm	1700N, at 38.5mm	554.438	No crack
B	2842N, at 22mm	623N, at 47.5mm	532.875	Cracked
C	2410N, at 12mm	295N, at 19.5mm	451.875	Cracked
A2	1418N, at 20mm	107N, at 35mm	265.875	No crack
B2	3460N, at 24mm	947N, at 48mm	648.375	No Crack
C2	3040N, at 23mm	805N, at 46mm	570	No Crack

4.2 Tensile Tests

This section presents the results that were obtained from the tensile testing machine. It should be noted that the specimens format used in section 4.1 was also followed in this section as well. The data logged in this section was used to calculate the corresponding specimens ultimate tensile stress (UTS) and the percentage elongation (equation (1) and (2)) and the corresponding calculations are included in Appendix G.

4.2.1 Processed and Unprocessed TIG results

Figure 4.2.1(a) demonstrate the post-tensile test unprocessed TIG specimens. All the specimens failed at the center of the joint and the mode of failure looks brittle. It can also be observed that the failure occurred at the filler and there are no signs of slenderness on the joint hence classified as brittle failure [KumarSingh et al., 2018]. This kind of failure suggests that the joint was dominated by the filler hence the failure occurred on the filler. The post-tensile test for processed TIG specimens is shown in figure 4.2.1(b). The

position of failure varies with specimen and the failure did not occur at the centre like it happened with the unprocessed specimens. There are some minor signs of slenderness that are observed on the figure. This suggests that the mode of failure was almost ductile [Yuqing et al., 2017]. This also shows that the bondage between the two plates welded was improved post FSP.



Figure 4.2.1: (a) Post-tensile test TIG specimen.



Figure 4.2.1: (b) Post-test FSP-TIG specimen.

Figure 4.2.1(c) shows the graphical representation of tensile test results for the processed and unprocessed TIG welded joints. The notable trend shown in this figure is that the tensile strength of the processed and unprocessed specimen is lower in the beginning of the plates (A and A1) compared to those at the end of the plates (C and C1). It is assumed that this trend emerges from the initial instability of the welding or processing technique hence low tensile strength of the specimen cut from the beginning of the plate [Subbaiah et al., 2018; Shalina et al., 2018]. The ultimate tensile strength of the processed joint is higher than the unprocessed one and this is the case in all locations of the plate (A, B and C). This suggests that the unprocessed joint is more porous compared to the processed ones. The application of FSP reduces the porosity of the joint. The graphical representation of unprocessed TIG specimens reveals the brittleness failure while the processed ones display ductility.

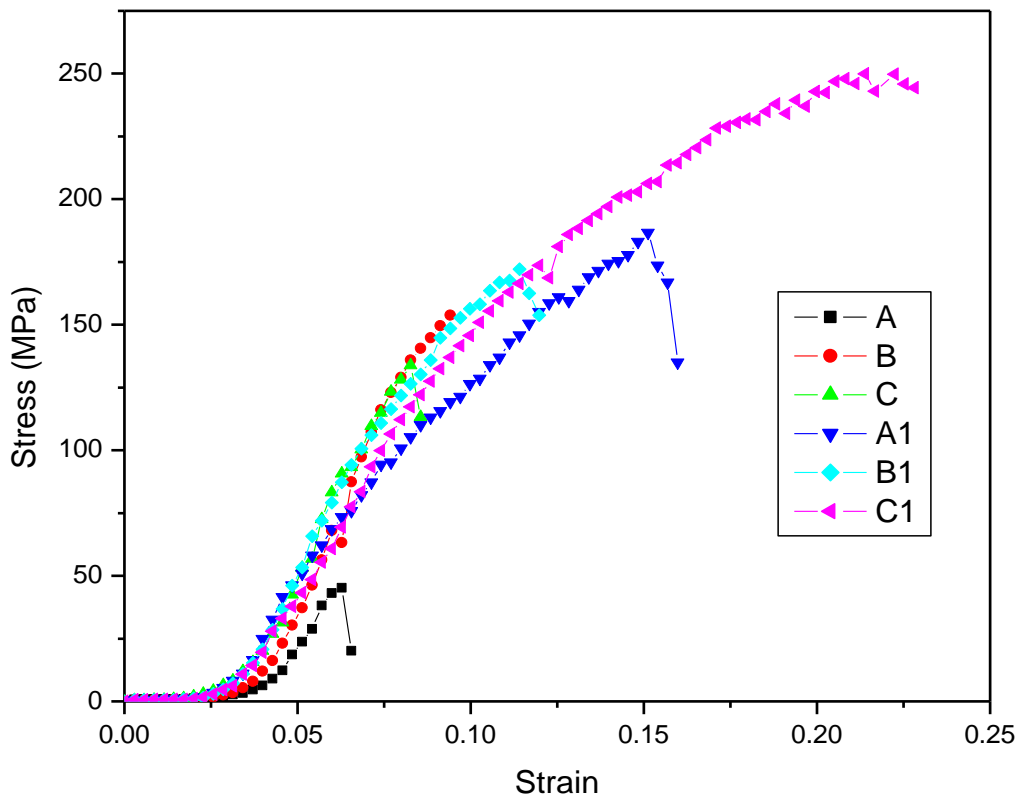


Figure 4.2.1: (c) Tensile stress – strain curves for processed and unprocessed TIG.

The numerical values associated with figure 4.2.1(c) are tabulated in Table 4.2.1. The numerical values are in agreement with the graphical representation of the tensile strength results. There is also a notable improvement on the percentage elongation of the processed joint compared to the unprocessed one. This suggests that the ductility of the material has improved. The stiffness of the unprocessed joint is lower than that of the base material while the one for processed is very close to that of the base material. This suggests that the unprocessed TIG welded joint is dominated with pores hence low stiffness [Gao et al., 2016].

Table 4.2.1: Processed and unprocessed TIG tensile weld joints results.

Sample	Proof Stress (MPa)	Ultimate Tensile Stress (MPa)	Elastic Young's Modulus (GPa)	Elongation (%)
A	38.220	46.028	15.343	6.56
B	68.111	153.75	51.25	9.41
C	53.139	133.833	36.171	8.56
A1	122.08	186.722	50.465	16
B1	93.421	172.167	46.532	12
C1	173.611	249.917	67.545	22.86

4.2.2 Processed and Unprocessed FSW

The post-tensile test specimens are shown in figure 4.2.2(a). All the specimens failed consistently at the centre of the joint. There are also some signs of slenderness at the failed location. This suggests that the failure mode is ductile. There is a consistent angular fracture that is observed on the fractured surfaces. This suggests the high stiffness on the joint. The processed FSW joint shown in figure 4.2.2(b) reveal similar behaviour with the unprocessed joint. However, the failure of the processed specimens occurred consistently away from the centre. This shows that the processed joint strength is close to the parent material.



Figure 4.2.2: (a) Post-test unprocessed FSW specimen.



Figure 4.2.2: (b) Post-test FSP-FSW specimen.

Figure 4.2.2(c) shows the graphical representation of tensile test results for the processed and unprocessed FSW welded joints. The trend noted with processed and unprocessed TIG welded joint is also noticed with FSW results. The only notable difference is that the tensile strength of the unprocessed FSW welded joint is higher than that of the unprocessed TIG welded joint [Liu et al. 2003; Ceshini et al., 2007]. The tensile strength of the processed FSW joint shows a clear increment along the plate while the unprocessed shows some fluctuations. This linear increment suggests that the porosity of the joint is getting reduced towards the end of the plate hence the improved ductility shown by percentage elongation. The numerical values tabulated in Table 4.2.2 are also in agreement with the graphical representation of data shown in figure 4.2.2.(c).

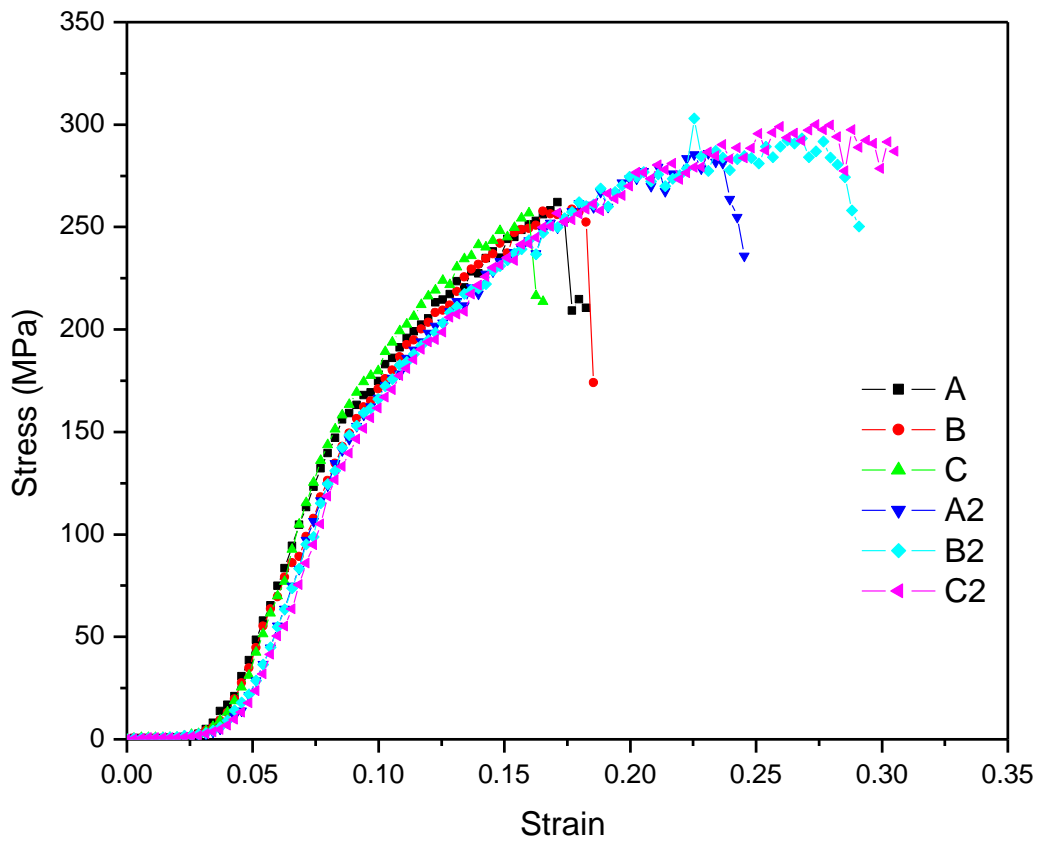


Figure 4.2.2: (c) Tensile stress – strain curves for processed and unprocessed FSW.

Table 4.2.2: Processed and unprocessed FSW tensile weld joints results.

Sample	Proof Stress (MPa)	Ultimate Tensile Stress (MPa)	Elastic Youngs Modulus (GPa)	% Elongation (%)
A	174.528	262.083	66.518	17.11
B	162.167	258.75	59.428	18.54
C	179.861	256.806	56.064	16.54
A2	139.722	286.028	70.833	24.5
B2	156.806	303.083	69.932	29.09
C2	118.611	299.944	69.407	30.52

4.3 Hardness Tests

This section presents the results that were obtained from the hardness tests for three unprocessed FSW, processed FSW, unprocessed TIG and processed TIG welded joint. Table 4.3.1 shows the results for the hardness test performed on the processed and unprocessed TIG welded joints, as well as processed and unprocessed FSW, welded joints. It is evident from the table that both processed and unprocessed TIG and FSW had high maximum HRB scale compared to the commercial AA5083 which is 53 HRB. This shows that the processed joints have high resistance towards deformation. The FSP hardness behaviour is in line with the hardness reported for wrought 5XXX series aluminium alloys, in which there is a marginal change in hardness between the stir zone and the base material [Verma et al., 2016; Zhang et al., 2012]. These results correlate with the tensile strength results presented in the previous sections (4.1 & 4.2). This also suggests that there is grain size refinement at the processed joint. The processed FSW is much higher than the processed TIG welded joint. This suggests that the grains of processed FSW are smaller than those of processed TIG ones (based on Hall-Patch relationship).

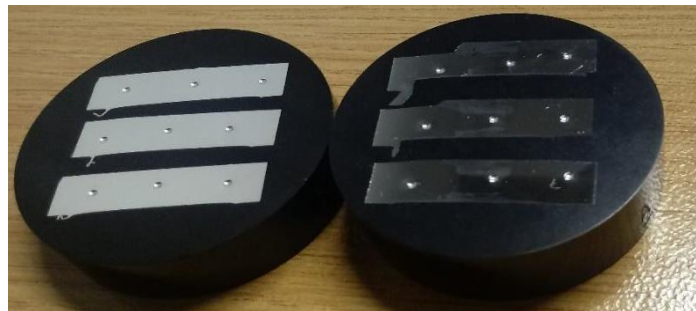


Figure 4.3: Hardness test post test samples.

Table 4.3.1: Hardness test results.

	Sample	HRB				HRB Maximum
		1	2	3	Average	
TIG	A	58.3	54.6	62.7	58.5	58.5
	B	59	54.9	61.9	58.6	
	C	59.6	55	60.9	58.5	
FSP-TIG	A1	58.8	61.0	60.2	60	60
	B1	57.9	58.7	57.3	58	
	C1	58.9	57.9	56.9	57.9	
FSW	A	59	58.7	59.3	59	58.7

	B	58.8	60	60.8	59.9	
	C	59.2	58.3	54.7	57.4	
FSP-FSW	A2	58.8	63.4	63.6	62	62
	B2	58.6	61	60.2	59.9	
	C2	61.7	60.9	62	61.5	

4.4 Macrostructure Tests

Figure 4.4.1 shows the macrostructure of an unprocessed TIG welded joint. There are few pores that are appearing on the joint but there were no cracks observed post welding. It is clear from the figure that the joint is dominated by the filler (the dark H-like structure) with no direct contact between the welded plates surface. It is assumed that the distinction between the welded plates and the filler together with the presence of pores on the joint contributes towards the joint weakness. Figure 4.4.2 shows the TIG welded joint after it has been processed. The onion ring is being observed and the filler cannot be clearly seen from the joint. There are no pores and cracks observed from the figure.

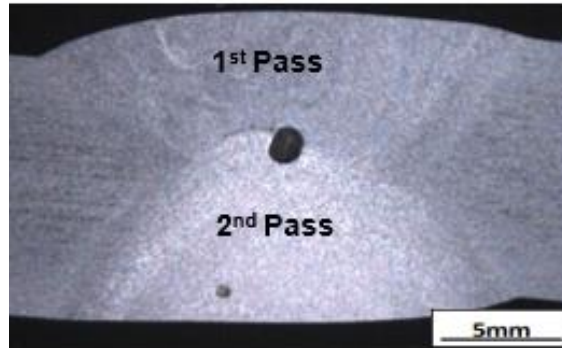


Figure 4.4.1: Unprocessed TIG welded 5083 alloy.

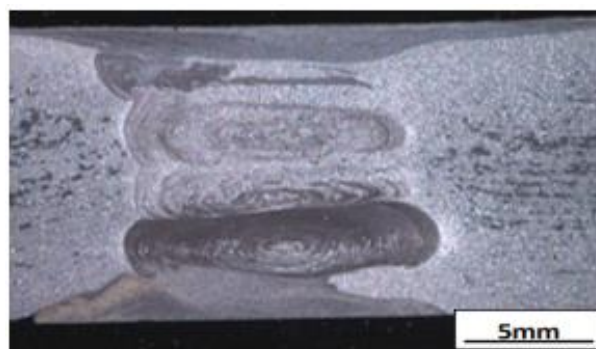


Figure 4.4.2: Processed TIG alloy macrostructure - onion ring.

The macrostructure of an unprocessed FSW joint is shown in Figure 4.4.3. The joint shows bonding without defects. The processed FSW, processed TIG and unprocessed FSW regions contained a special microstructure feature, “the onion ring” structure, which is sometimes called the banded structure [Krishnan, 2002]. The onion rings consist of concentric, elliptical rings located in the middle of the processed FSW, unprocessed FSW, and processed TIG nugget. The banded structure can also be observed in the top cross-section, and the space between each ring corresponds to the advance per revolution of the tool [Ciu et al., 2008]. The appearance of onion rings was due to a periodic particle density variation or grain size variation [Yang et al., 2004]. The processed FSW joint reveal elongated onion rings (see Figure 4.4.4) compared to the unprocessed. This suggests that the bonding between the plates is improved hence higher than the unprocessed joint.

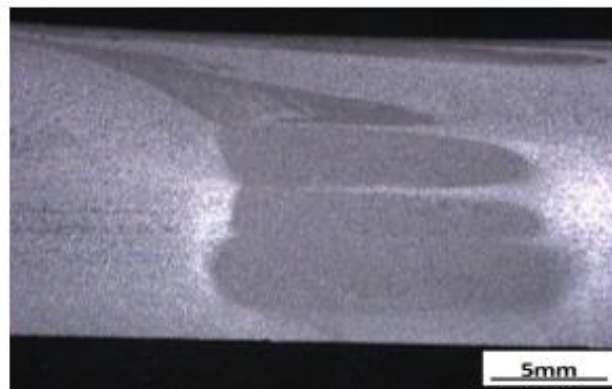


Figure 4.4.3: Unprocessed FSW joint.

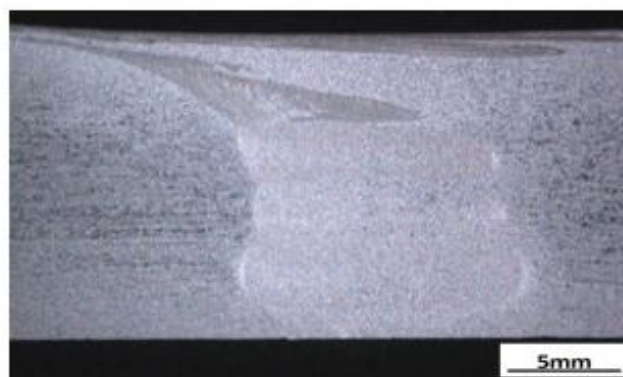


Figure 4.4.4: Processed FSW onion ring.

4.5 Microstructure Tests

Microstructure tests were performed to analyse the grain structure arrangements. Observations of the TIG welded joint plate were that there were no surface cracks and discontinuation detected. The spatter found were very small in size. Figure 4.5.1 show micrograph of unprocessed TIG welded joints. The figure consisted of the dark dendrites with fine precipitates of Mg_2Al_3 , this is a common phenomenon with filler wire ER 5356 microstructure [Stevens 2000].

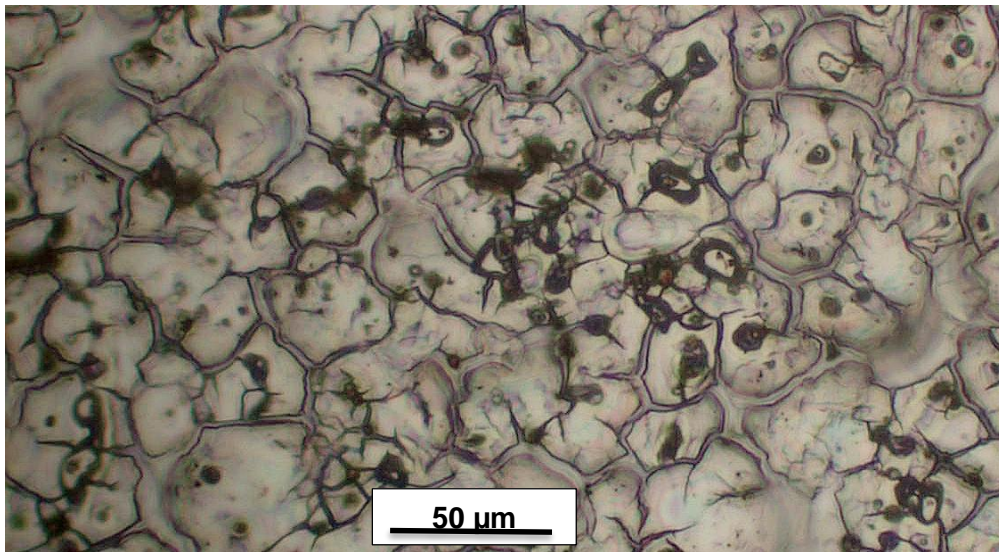


Figure 4.5.1: Unprocessed TIG welded microstructure.

It should be noted that all the micrographs were taken only on the nugget zones where the onion rings were found. Figure 4.5.2 presents processed TIG micrograph. The application of FSP on the TIG welded joints resulted in very fine grain structure with distinguished boundary layers in comparison to the unprocessed one. There is a significant reduction of pores on the processed TIG welded joint. Processed FSW grain structure illustrated in figure 4.5.4 showed finer grains in comparison to unprocessed FSW grain structure shown in figure 4.5.3. The grain refinement in friction stir processed specimens is assumed to be caused by the intense plastic deformation of metal by the rotating tool in stir zone resulting in the breaking of all micro-constituents and dynamic recrystallization [Subramani et al., 2019; Prosgolitis et al., 2018].

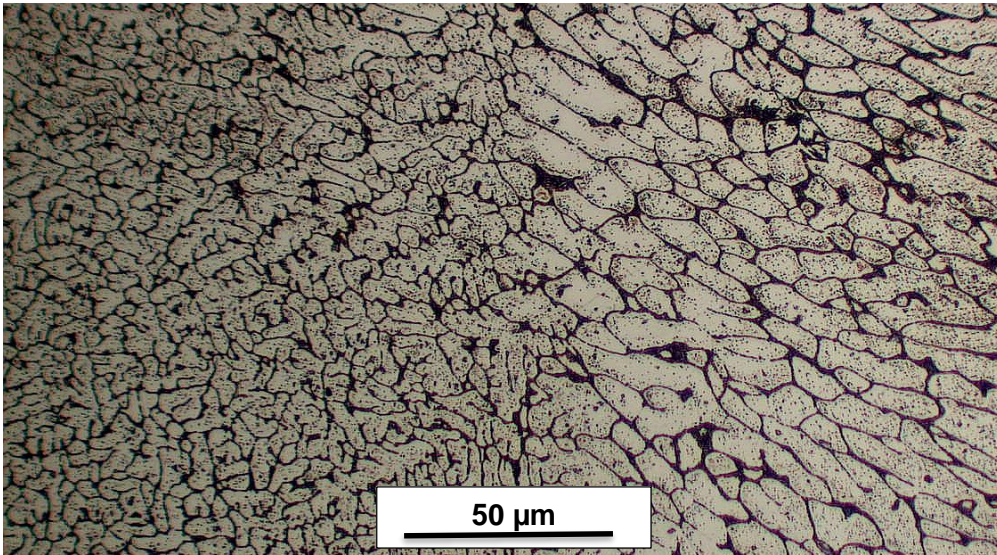


Figure 4.5.2: Processed TIG alloy microstructure, nugget zone.

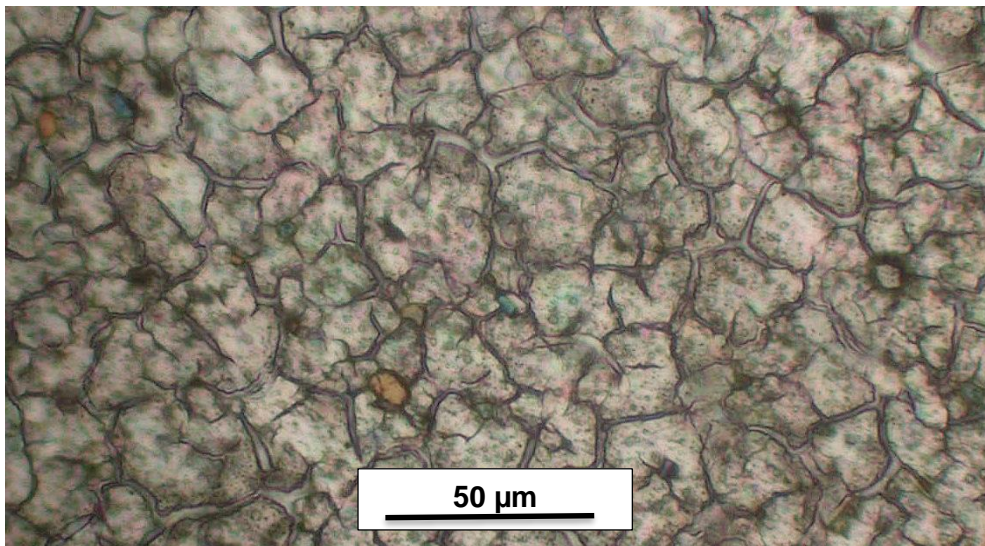


Figure 4.5.3: Unprocessed FSW microstructure; nugget zone.

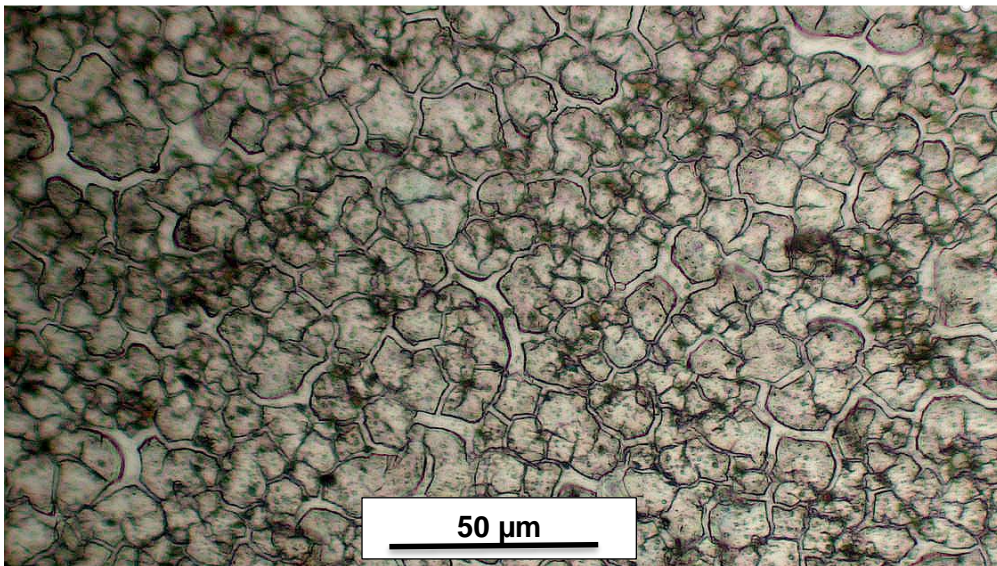


Figure 4.5.4: Processed FSW Alloy Microstructure; nugget zone.

The microstructural grain sizes were measured on the onion ring region for unprocessed FSW and TIG, and processed FSW and TIG. The 50 μm scale and objective 20x were used for the analysis. Three measurements were performed on the joint hence number 1 to 3 in Table 4.5.1. The table also shows the mean grain sizes and standard deviations. The unprocessed TIG mean grain size is 10.78 μm and the processed one is 7.177 μm . The mean grain size for the unprocessed FSW joint is 8.67 μm while the processed one is 4.62 μm . The grain refinement of the friction stir processed welded joints is in agreement with the Hall–Petch relation which predicts that the grain size decreases with an increase in the UTS [Hassan, 2018; Zhang et al., 2012].

Table 4.5.1: Grain sizes measured.

Technique	Diameter (μm)				
	1	2	3	Mean	Standard Deviation
Base	18.63	15.63	17.16	17.14	1.50
FSW	8.57	8.20	9.20	8.657	0.362
FSP-FSW	4.74	4.44	4.68	4.62	0.127
TIG	10.96	10.30	11.08	10.78	0.249
FSP-TIG	7.010	7.520	7.000	7.177	0.125

4.6 Scanning Electron Microscopy (SEM) Tests

The post-test for tensile test specimens were then cut out on the fracture points as shown in figure 4.6.1 for examination. The cut-off pieces in figure 4.6.2(a), (b), (c) and (d) were

then taken to the SEM for the analysis of the nature of the fracture.

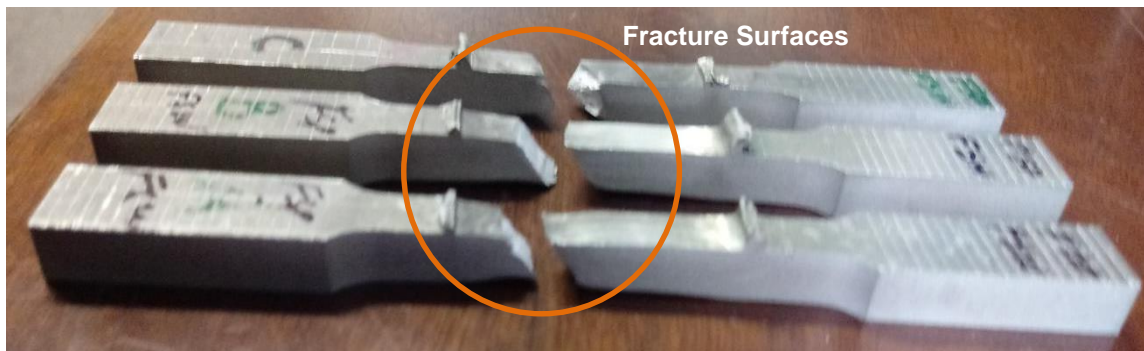


Figure 4.6.1: Fracture surfaces.

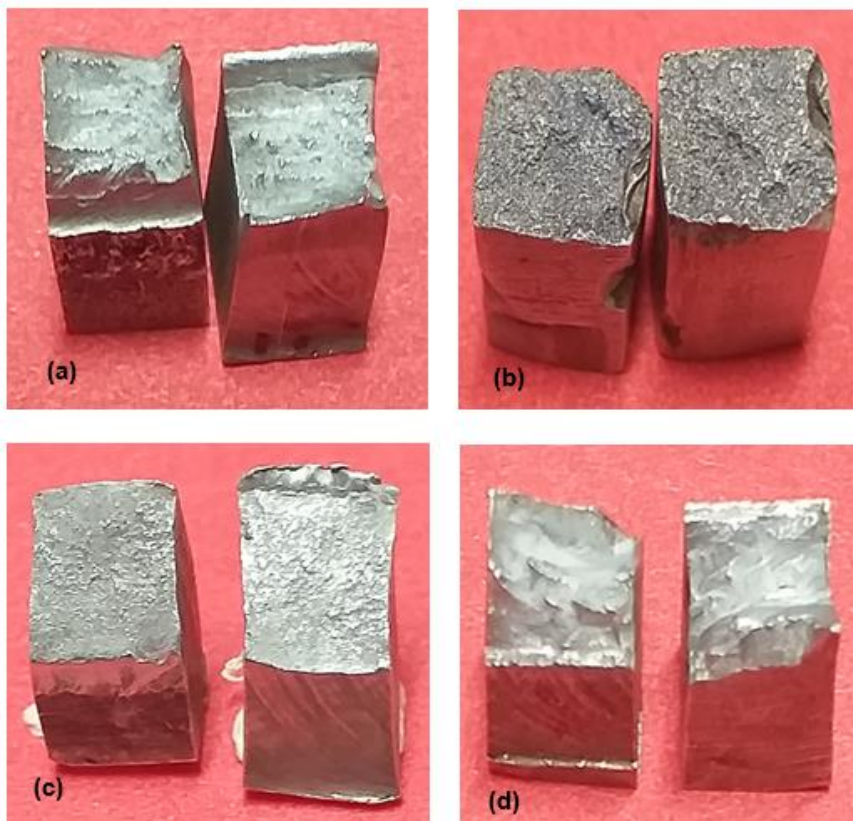


Figure 4.6.2: SEM Specimens; (a) Unprocessed FSW; (b) Unprocessed TIG; (c) Processed FSW; (d) Processed TIG.

Figure 4.6.3 reveals the SEM micrograph of the fractured surfaces for the unprocessed and the processed TIG and FSW joint specimens. The unprocessed TIG welded joint in Figure 4.6.3(a) show some rough fracture surface with some notable pores. There are no notable dimples formed on the fracture surface. This kind of observation suggests that the TIG welded joint had a brittle failure. On the other hand, there is a notable amount of

dimples formed on the surface of the other three fracture surfaces (Figure 4.6.3 a, c and d). There are no notable pores on the fracture surfaces of these three. These observations suggest a ductile failure of the unprocessed FSW, processed TIG and FSW joints. The SEM results show some correlation with the results presented in the previous sections of this chapter.

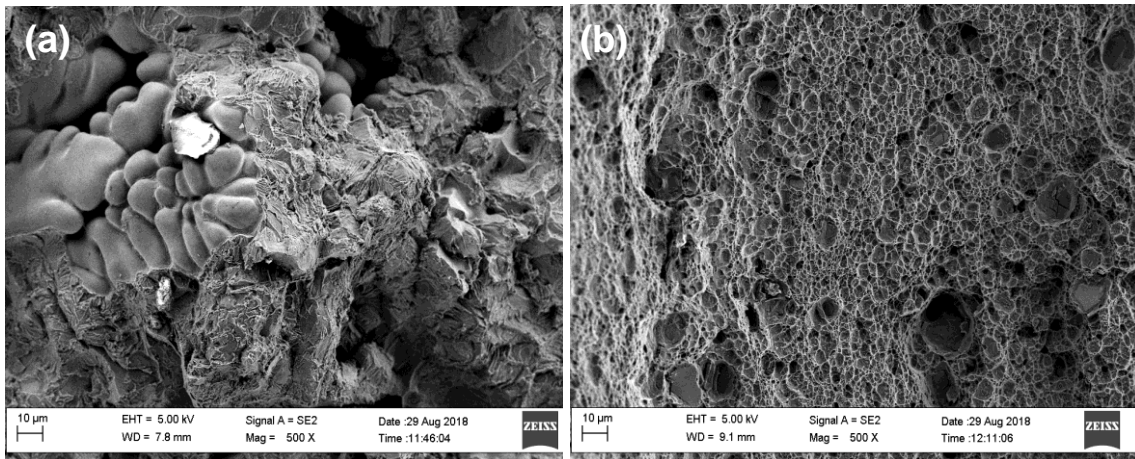


Figure 4.6.3: SEM Photos; (a) TIG, and (b) FSP-TIG.

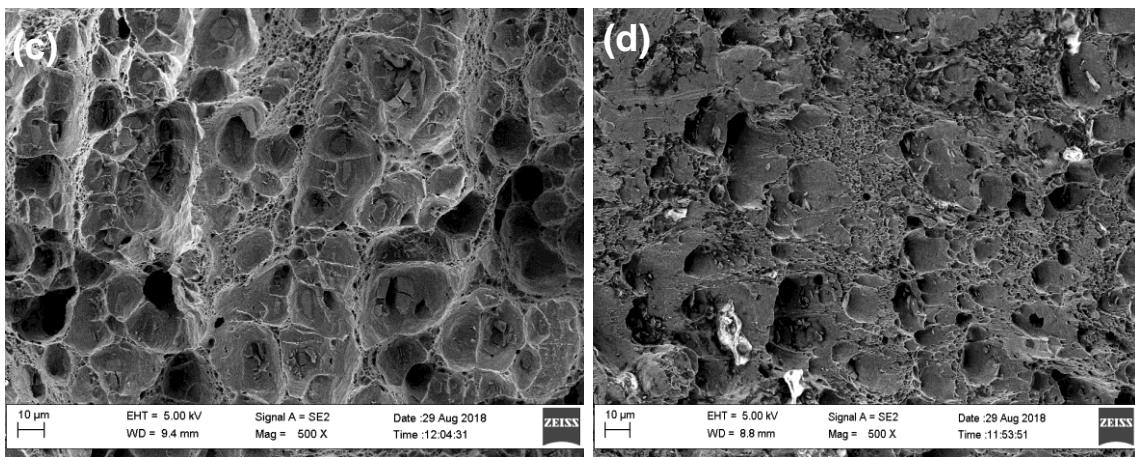


Figure 4.6.3: SEM Photos; (c) FSW, and (d) FSP-FSW.

4.7 Comparison of Mechanical Properties

Table 4.7 is showing mechanical properties of friction stir processed FSW in comparison with friction stir welding, as well as for TIG and friction stir processed TIG. From the results, it is evident that friction stir processing strengthens the bond of the aluminium 5083 joint. This judged from the increase in numerical values associated with the corresponding tests. The practical results for friction stir processing AA5083 were then

compared to the commercial material, the FSP was found to have higher values compared to the commercial material. There is a clear distinction between the processed and the unprocessed TIG welded joints. The processed joints for both TIG and FSW showed an improved ductility compared to unprocessed ones. This also is in agreement with the improvement seen from tensile test results.

There is no major difference observed from the results obtained from the root of the specimens. The microstructural results showed the refinement of grains in friction stir processed TIG and FSW in comparison with plain TIG and FSW. The unprocessed TIG joints yielded the maximum tensile stress of 111.204MPa while processed TIG produced the average of 202.935MPa. There is a notable ductility improvement on the processed joints compared to the unprocessed one. The stiffness of the processed joint is close to the stiffness of the base material (commercial material or parent material). This indicates that the FSP improved the mechanical properties of the TIG welded joint.

The average tensile strength for unprocessed FSW joints was found to be 259.213MPa while processed FSW yielded the maximum UTS of 296.35MPa. The average percentage elongation of unprocessed FSW joints was found to be 17.40% while 28.05% corresponded with the average elongation of the processed FSW joint. This elongation improvement suggests an improved ductility of the processed FSW joint. The stiffness of the processed joint is close to the stiffness of the base material. This indicates that the FSP has improved the mechanical properties of the FSW welded joint.

Table 4.7: Practical mechanical properties.

	Hardness HRB	Ultimate Tensile Strength (MPa)	Flexural Strength (Face) (MPa)	Flexural Strength (Root) (MPa)	Yield Strength (MPa)	Young's Modulus (GPa)	% Elongation
5083	53	275-350	-	-	125	70.3	16
FSW	58.7	259.213	648.438	513.063	138.38	60.67	17.40
FSP-FSW	62	296.35	676.125	494.75	172.185	70	28.05
TIG	58.5	111.204	328.375	295.813	53.157	34.255	8.177
FSP-TIG	60	202.935	465	407.625	129.7	54.847	16.9

CHAPTER FIVE

CONCLUSIONS

This chapter concludes about the main key points of the study. It also highlights points of improvement when one wants to take the study forward.

The analysis of the processed and unprocessed TIG and FSW welded joints was successfully carried in this study. There were no special conditions considered in carrying out this study. The study was based on finding out whether friction stir processing improves the mechanical properties of TIG and FSP welded joints. Based on the findings of this study, the following conclusions were drawn.

The results show that the mechanical properties of the processed TIG and FSW welded joints are higher than the unprocessed joints of the same welding technique. The unprocessed TIG welded joint was found to be mechanically weaker compared to the unprocessed FSW joints. The weakness was due to the porosity observed microstructurally and microstructurally. It was also observed that the processed TIG welded joints were mechanically higher than the unprocessed TIG welded joints. This highness was due to the microstructural changes that were induced by the employment of FSP technique. The similar trend was also observed with the FSW welded joints. The numerical analysis of the processed TIG welded joints are comparatively similar to the ones for the unprocessed FSW welded joints. The processed TIG welded joints share some microstructural similarities with the unprocessed FSW welded joints. This includes the onion rings observed at the nugget region.

The application of FSP technique brought about the reduction of grain sizes and homogenous arrangement around the processed region. It was also observed that the numerical and graphical analysis of the processed FSW was found to be higher than all the other three joints (unprocessed TIG, processed TIG and unprocessed FSW joints). This notable behaviour is suggested to be caused by the fact that FSW and FSW are similarly so the application of FSP to the FSW welded joint sounds like the repeated FSP. It was also observed that there is a brittleness failure occurring in almost all the specimens. This behaviour emerges from the parent material. There was an unmatched improvement noted between the unprocessed TIG welded joint and the processed TIG

welded joint. This study has demonstrated that the FSP technique can be used as a technique to improve the mechanical properties of the TIG and FSW welded joints.

RECOMMENDATIONS

It is recommended that a future study considers the comparative study of dissimilar aluminium alloys of the processed TIG and FSW, and unprocessed TIG and FSW. It would be better to also look at the impact of controlling rate of the joint (processed and unprocessed). The fatigue test analysis is recommended for future study.

REFERENCES

Abdulmalik, S. S., Ahmad, R. and Usman, O. Y. 2018. Microstructure and Tensile Properties of Friction Stir Processed Al-Si Alloy. Saudi J. Eng. Tech., Vol-3, Iss-9 (Sep, 2018): 593-597.

Abdel-Aziz, A. I., AbouTaleb, A. S. A., El-Baradie, Z. M. and Farahat, A. I.Z. 2018. Effect of Friction Stir Processing on the Microstructure and Mechanical Properties of A384 Aluminum Alloy. Key Eng. Mat. Vol. 786, pp 23-36.

Ahmad, I., and Arya, S. (2018). To Study the Micro-Structural of Aluminum Alloy AA-6061 Welded Using TIG Welding Process at Different Welding Current. 395–403.

Axenics. 2017. Exploring the Advantages and Disadvantages of TIG Welding. <https://axenics.com/blog/exploring-advantages-disadvantages-tig-welding>. [10 July 2018].

Beamish, K.A. and Russell, M.J. 2010. 'Relationship between the features on an FSW tool and weld microstructure. *8th International Symposium on Friction Stir Welding*. Timmendorfer Strand, Germany, TWI.

Cetinel, H. and Mehmet, A. 2014. Microstructure and Mechanical Properties of AA 5083 and AA 6061 Welds Joined with AlSi5 and AlSi12 Wires. Manisa, Turkey. Hanser-Elibrary Journal. Volume 56, Issue 10 (October 2014).

Cevik, E., Sun, Y. and Ahlatci, H. (2012). Effect of Peak-Aged Heat Treatment on Corrosion Behavior of the AA6063 Alloy Containing Al3Ti. Archives of Metallurgy and Materials, 57(2), 469–477.

Ceschini, L., Borome, I., Mina, M., Morria, A. and Tarterinia, F. 2007. Effect of friction stir welding on microstructure, tensile and fatigue properties of the AA7005/10 vol.%Al₂O₃p composite. Composites Science and Technology. Vol. 67, iss. 3–4, pp. 605-615.

Chan, C. Y. 2011. Friction Stir Processing of Aluminium-Silicon Alloys. Thesis Degree of Doctor of Philosophy. University of Manchester.

Chainarong, S., Muangjunburee, P. and Suthummanon, S. 2014. Friction Stir Processing of SSM356 Aluminium Alloy. Science Direct. Procedia Engineering 97 (2014) 732 – 740.

Chandu, K.V.P.P., Rao, E. V., Rao, S. A. and Subrahmanyam B. V. 2014. The Strength of Friction Stir Welded Aluminium Alloy 6061. IJRMET Vol. 4, Issue SPL - 1, Nov 2013 – April 2014.

Chaudhari, R., Parekh, R., and Ingle, A. (2014). Reliability of Dissimilar Metal Joints using Fusion Welding: A Review. 98–104. <https://doi.org/10.15242/iie.e0114050>

Chen, Z. 2014. Microstructure characterization, mechanical properties, and corrosion resistance of FSW AA5086. M. Sci. Mech. Eng.

Ćurković, L. 2010. Flexural strength of alumina ceramics: Weibull analysis. Transactions of FAMENA 34(1):13-19.

Cui, G. R., Ma, Z.Y. and Li S. X. 2008. Periodical plastic flow pattern in friction stir processed Al–Mg alloy. Scri. Mat., Vol. 58, pp. 1082-1085.

Fadhel, A., Hashim, R., and K. Salim, K. and Basheer, H. K. 2015. Effect of Friction Stir Processing on (2024) Aluminum Alloy. IJIRSET, Vol. 4, Issue 4, 2015, pp. 1822-1829.

Davis, J. R. (2001). Light Metals and Alloys. *Alloying: Understanding the Basics*, 351–416. <https://doi.org/10.1361/autb2001p351>

Darras. B. M. 2005. Experimental and Analytical Study of Friction Stir Processing. Thesis Masters. University of Kentucky. [06 February 2018].

Freeney, T. A. 2007. Friction stir processing of cast magnesium alloys. University of Missouri-Rolla. Master of Science in Materials Science and Engineering.

Gao, Y., Nakata, K., Nagatsuka, K. T., Matsuyama, T., Shibata, Y. and Amano, M. 2016. Microstructures and mechanical properties of friction stir welded brass/ steel dissimilar lap joints at various welding speeds. Mater. Des. 90, 1018–1025.

Gomathisankar, M., Gangatharan, M. and, P. 2018. A Novel Optimization of Friction Stir Welding Process Parameters on Aluminum Alloy 6061-T6. Materials today: Proceedings. Volume 5, Issue 6, Part 2, 2018, Pages 14397-14404

Gopan, V., Sreekumar, P. S., Chandran, J. P., Vijay, W. and Sanjay Kumar. M. S.2018. The Effect of Various Process Parameters On FSP of Aluminium Alloys. Materials Today: Proceedings 5 (2018) 13674–13681.

Grill, T. 2017. Friction Stir Welding – Working Principle, Advantages, Disadvantages with Application. The Welding Master. <http://www.theweldingmaster.com/friction-stir-welding/>. [09 July 2018].

Hassan, H. A., 2018. Comparative study of mechanical properties aluminum alloy 5052-O welded by TIG and FS processes. International Journal Mechanical Engineering Technology, p. 131–140.

Iwaszko, J., Kudła, K., Fila, K. and Strzelecka, M. 2016. The Effect Of (FSP) On The Microstructure And Properties Of Am60 Magnesium Alloy. Arch. Metall. Mater., Vol. 61 (2016), No 3, p. 1555–1560.

Krishnan, K. N. 2002. On the formation of onion rings in friction stir welds. Mat. Sci. and Eng. A, Vol. 327, pp. 246-251.

Kumar, A. R., Varghese, S. and Sivapragash, M. 2012. A Comparative Study of the Mechanical Properties of Single and Double Sided Friction Stir Welded Aluminium Joints. Procedia Engineering 38 (2012) 3951 – 3961.

Kumar-Singh, S., Tiwaria, R. M., kumara, A. Kumar, S., Murtaza, Q. and Kumar, S. 2018. Mechanical Properties and Micrstructure of Al-5083 by TIG. Science Direct. Materials Today: Proceedings 5 (2018) 819–822.

Liu, H. J., Fujii, H., Maeda, M. and Nogi K. 2003. “Friction Stir Welding of AA5083 Aluminum Alloy. Transactions of Nonferrous Metals Society of China. Vol. 13, pp. 14.

Liu, H. J., Fujii, H., Maeda M. and Nogi, K. 2013. Mechanical Properties of Friction Stir Welded Joints of 1050 – H24 Aluminium Alloy. Science and Technology of Welding and Joining : Volume 8, Issue 6.

Mahoney, M. W. and Lynch, S. P. 2006. Friction Stir Processing. Defence Science and Technology Organisation, Melbourne, Australia.

Mcnelley, T. R. 2011. Friction Stir Processing (FSP): Refining Microstructures and Improving Properties. Revista De Metalurgia. Vol. 46, pp. 149-156.

Mishra, R. S., Mahoney, M. W., McFaden, S. X., Mara, N. A. and Mukherjee, A. K. High strain rate superplasticity in a friction stir processed 7075 Al alloy. United States: N. p., 1999.

Mishra, R. S. and Ma, Z. Y. 2005. Friction Stir Welding and Processing. Department of Materials Science and Engineering, University of Missouri, Rolla, MO 65409, USA Institute of Metal Research, Chinese Academy of Sciences, Shenyang 110016, China.

Mohan, P. 2014. Study The Effects of Welding Parameters On TIG Welding of Aluminium Plate. Thesis: Master of Technology in Production Engineering. Department of Mechanical Engineering National Institute of Technology Rourkela -769 008 (India).

Munoz, A. C., Rückert, G., Huneau, B., Sauvage, X., Munoz, A. C., Rückert, G. and Marya, S. (2017). Comparison of TIG welded and friction stir welded Al-4. 5Mg-0. 26Sc alloy To cite this version : HAL Id : hal-01005980 Comparison of TIG welded and friction stir welded. 0–7.

Murthy, V. and Rajaprakash, B. M. 2018. Investigation on the effect of friction stir processing on tribological and mechanical properties of Al 7075-T651 alloy. <https://aip.scitation.org/doi/abs/10.1063/1.5029625>. AIP Conference Proceedings 1943, 020049 (2018).

Northeast Precision Machinery. 2019. Cosen AH-250H Automatic Bandsaw. <http://www.northeastprecision.com/cosen-ah-250h-band-saws.html>.

[6 March 2019].

Nur, R., Sultan, A. Z. and Suyuti, M. A. 2017. Mechanical Properties On Friction Stir Welding of Aluminium Alloy 5052. Journal of Engineering and Applied Sciences. VOL. 12, NO. 15. Asian Research Publishing Network (ARPN).

Paik, J. 2009. Mechanical Properties of Friction Stir Welded Aluminium Alloys 5083 and 5383. Inter J Nav Archit Oc Engng. 1:39- 49. Korea. [04 January 2018].

Palanivel, R., Koshy Mathews, P. and Murugan, N. 2011. Development of mathematical model to predict the mechanical properties of friction stir welded AA6351 aluminum alloy. Journal of Engineering Science and Technology Review, vol.4, no.1, pp. 25-31.

Park, M. (2015). Aluminum and Aluminum Alloys Guide Aluminum and Aluminum Alloys. ASM International.

Patil, C. P. and Shelke, R. D. 2016. Experimental Investigation and Optimization of Welding Parameters On TIG Welding of AA7005. IOSR Journal of Mechanical and Civil Engineering (IOSR-JMCE), Volume 13, Issue 2 Ver. II (Mar. - Apr. 2016), PP 48-54.

Peel, M.J. 2005. The friction-stir welding of dissimilar aluminium alloys. The University of Manchester, *Doctor of Philosophy Thesis*.

Pradeep, S., Sharma, S. K. and Pancholi, V. 2012. Microstructural and Mechanical Characterization of Friction Stir Processed 5086 Aluminum Alloy. Materials Science Forum Vol. 710 (2012) pp 253-257. Trans Tech Publications, Switzerland.

Prosgolitis, C. G., Lambrakos, S. G., and Zervaki, A. D. 2018. Phase-field modeling of nugget zone for a AZ31-Mg-Alloy friction stir weld. Journal of Material Engineering and Performance. Vol., 27, iss. 10, pp. 5102–5113.

Ramakrishna, M. V. A. and Mahender, T. 2017. Investigation of Friction Stir Welding Parameters of 5083 Aluminum Alloy by Taguchi Method. International Journal of Engineering Technology Science and Research IJETSRS. ISSN 2394 – 3386, Volume 4, Issue 12.

Rao, C. M. and Rao, K. M. 2017. Friction Stir Welding of Aluminium Alloys 6061- To-6061 Similar Metals. *International Journal of Mechanical Engineering and Technology (IJMET)* Volume 8, Issue 1, January 2017, pp. 264–269, Article ID: IJMET_08_01_029.

Resan, K. K., Takhakh, A. M. and Salman, A. A. 2014. Effect of Friction Stir Processing (FSP) to the Mechanical Properties of 7075 Aluminium Alloys Plates Welded by Friction Stir Welding. *Journal of Engineering and Development*, Vol. 18, No.5, September 2014, ISSN 1813- 7822.

Rogers, N. 2018. The remarkable Abilities of Wire EDM. *TechSpec*. [2018-05-21].

Saini, N., Dwivedi, D. K., Jain, P. K. and Singh. H. 2015. Surface Modification of Cast Al-17%Si Alloys using Friction Stir Processing. *Procedia Engineering* 100 (2015) 1522 – 1531.

Salman, A. A., Takak, A. M. and Resan, K. K. 2016. Enhancements of mechanical Properties of Friction Stir Welding for 6061 Aluminium Alloy by FSP Method. Msc Thesis. Al-mustansiriyah University / college of Engineering / materials engineering department.

Sarma, B. 2018. Friction stir welding of thin aluminium alloy plates using milling machine: a basic compatibility study. *IOP: Materials Science and Engineering* 377 (2018) 012012 doi:10.1088/1757-899X/377/1/012012.

Sanusi, K. O. and Akinlabi, E. T. 2017. Friction-stir processing of a composite aluminium alloy (aa 1050) reinforced with titanium carbide powder. University of Johannesburg, Department of Mechanical Science, Auckland Park Kingsway Campus, Johannesburg 2006, South Africa. *Materiali in Tehnologije/Materials and Technology (1967–2017) – 50 Let/50 Years*.

Shalina, M. and Hiten, M., 2018. Experimental analysis on effect of tool transverse feed, tool rotational speed and tool pin profile type on weld tensile strength of friction stir welded joint of AA 6061. *Mater. Today: Proc.* 5 (1), 487–493.

Singh, K., Singh, G. and Singh, H. 2018. Investigation of microstructure and mechanical properties of friction stir welded AZ61 magnesium alloy joint. *Journal of Magnesium and Alloys* Volume 6, Issue 3, September 2018, Pages 292-298.

Singh, G., Singh, F. and Singh, H. 2015. A Study of Mechanical Properties on TIG Welding at Different Parameters with and without use of Flux. *HCTL Open International Journal of Technology Innovations and Research (IJTIR)* <http://ijtir.hctl.org> Volume 16, July 2015 e-ISSN: 2321-1814, ISBN (Print): 978- 1-943730-43-8.

Sinhmar, S., Dwivedi, D. K. and Pancholi, V. 2014. Friction Stir Processing of AA 7039 Alloy. *International Conference on Production and Mechanical Engineering (ICPME'2014)* Dec. 30-31, 2014 Bangkok, Thailand.

Stevens, R. H. 2000. *ASM Handbook Metallography and Microstructures*, ASM Int., USA, vol. 9, p. 362.

Subbaiah, K., Geetha, M., Shanmugarajan, B., Koteswara and Rao, S. R., 2012. Comparative evaluation of tungsten inert gas and laser beam welding of AA5083-H321. *Sadhana* 37(5), 587–593.

Subramanian, C. 2016. A Study of Microstructure and Mechanical Properties of Aa7075 Aluminium Alloy by Using Friction Stir Welding. *Journal of Chemical and Pharmaceutical Sciences*. Volume 9 Issue 4.

Subramani, V., Jayavel, B., Sengottuvelu, R. and Lazar, P. J. L. "Assessment of microstructure and mechanical properties of stir zone seam of friction stir welded magnesium AZ31B through Nano-SiC," *Mater.*, vol. 12, iss. 1044, pp. 1-19, 2019.

Sun, N. and Apelian, D. 2009. Microstructural Modification of A206 Aluminium via Friction Stir Processing. 4th LMT Conference, Queensland, Australia, 2009 *Materials Science Forum*, Vol. 618-619, p361-364, 2009.

Sun, N. 2009. Friction Stir Processing of Aluminium Alloys. Master of Science Thesis. Lexington, Kentucky.

Sun, N. 2012. Friction Stir Processing of Aluminum Alloys. Degree of Doctor of Philosophy, Material Science & Engineering. Worcester Polytechnic Institute.

Sun, N., Jones, W.J. and Apelian, D. 2018. Friction Stir Processing of Aluminum Alloy A206: Part II—Tensile and Fatigue Properties. *International Journal of Metalcasting*, 1-11.

Totten, G. E., and Mackenzie, D. S. (2003). *Handbook of Aluminum, Volume 1: Physical Metallurgy and Processes*. Marcel Dekker, INC. New York, Basel.

Vázquez, F. G., Arista, B. V, Muñoz, R., Ortiz, J. C., García, H. H. and Acevedo, J. 2016. The Role of Friction Stir Processing (FSP) Parameters on TiC Reinforced Surface Al7075-T651 Aluminium Alloy. Universidad Autónoma de Coahuila, Facultad de Ingeniería, Arteaga, Coahuila, México.

Verma, S., Gupta, M., and Misra, J. P., 2016. *Friction stir welding of aerospace materials: A state of art review*, Chapter 13 in DAAAM International Scientific Book, 135-150, B. Katalinic (Ed.). Published by DAAAM. International, ISBN 978-3-902734- 09-9, ISSN 1726-9687, Vienna, Austria.

Vyas, A. H. and Patel, R. M. 2017. A Review Paper on TIG Welding Process Parameters. *IJSRD - International Journal for Scientific Research & Development* | Vol. 5, Issue 02, 2321-0613.

Xuebao, H. 2014. Microstructure and mechanical properties of 5083 aluminum alloy joint by TIG welding. *Transactions of the China Welding Institution* 35(1):37-40.

Yang, B. and Yan, J. 2004. Sutton and A.P. Reynolds, Banded microstructure in AA2024-T351 and AA2524-T351 aluminium friction stir welds: Part I. *Metallurgical Studies. Mat. Sci. and Eng. A*, Vol. 364, pp. 55-65.

Yiqing, M., Liming, K., Fencheng, L. Yuhua C, and Li X., 2017. Effect of tool pin-tip profiles on material flow and mechanical properties of friction stir welding thick AA7075-T6 alloy joints. *The International Journal of Advanced Manufacturing Technology*. Vol. 88, 949-960.

Yue, Y., Wang, G., Yang, K., Wu, B. and Yan, D. 2018. Friction stir butt welding thin aluminum alloy sheets. *The International Journal of Advanced Manufacturing Technology* (2018) 96:3139–3147.

Zhang, Y.N., Cao, X., Larose, S. and Wanjara, P. 2012 Review of tools for friction stir welding and processing. *Canadian Metallurgical Quarterly* 2012 VOL 51 NO 3.

APPENDICES

APPENDIX A

Aluminium Plate

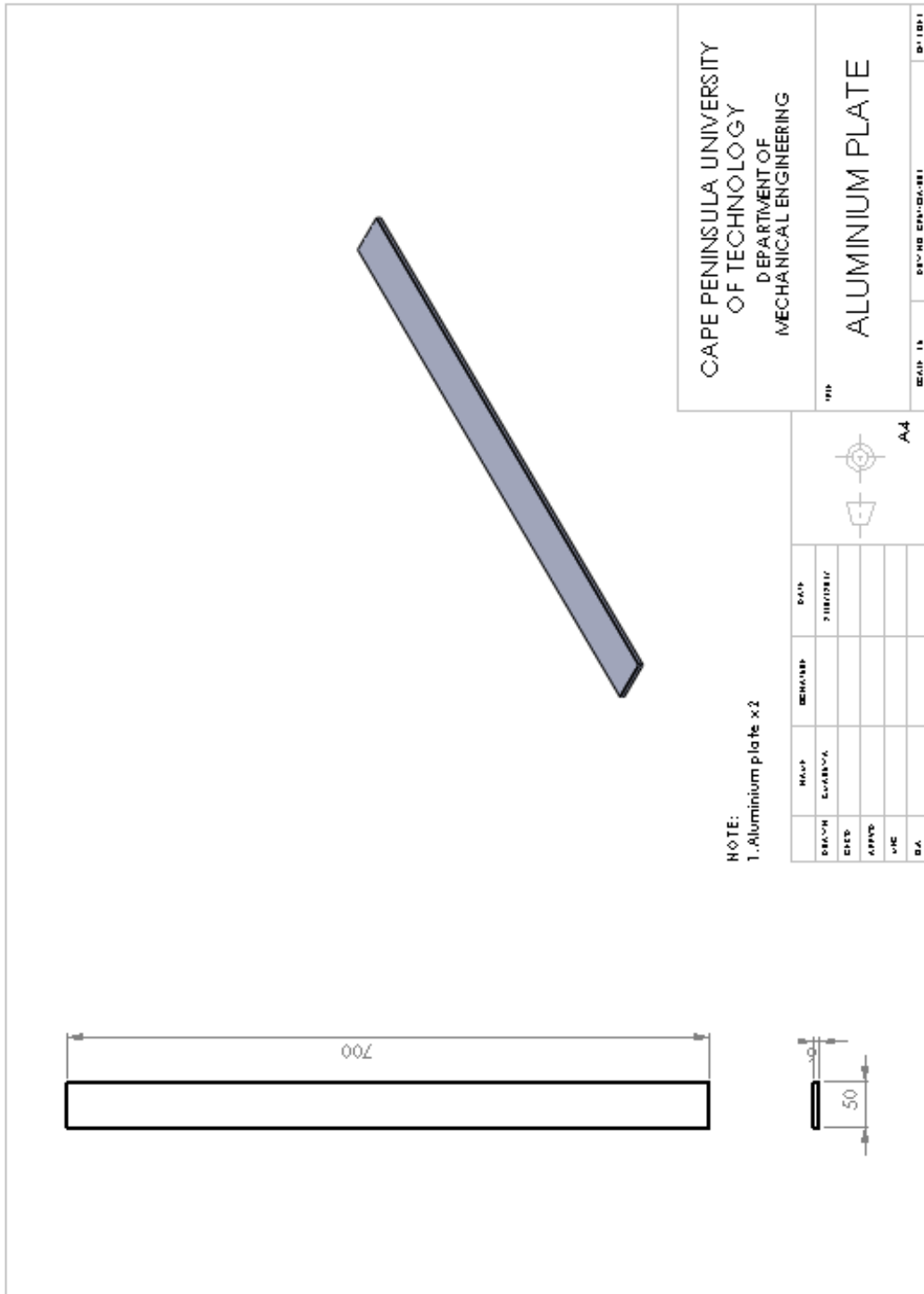


Figure A1: Aluminium Plate.

APPENDIX B

Pin Drawing

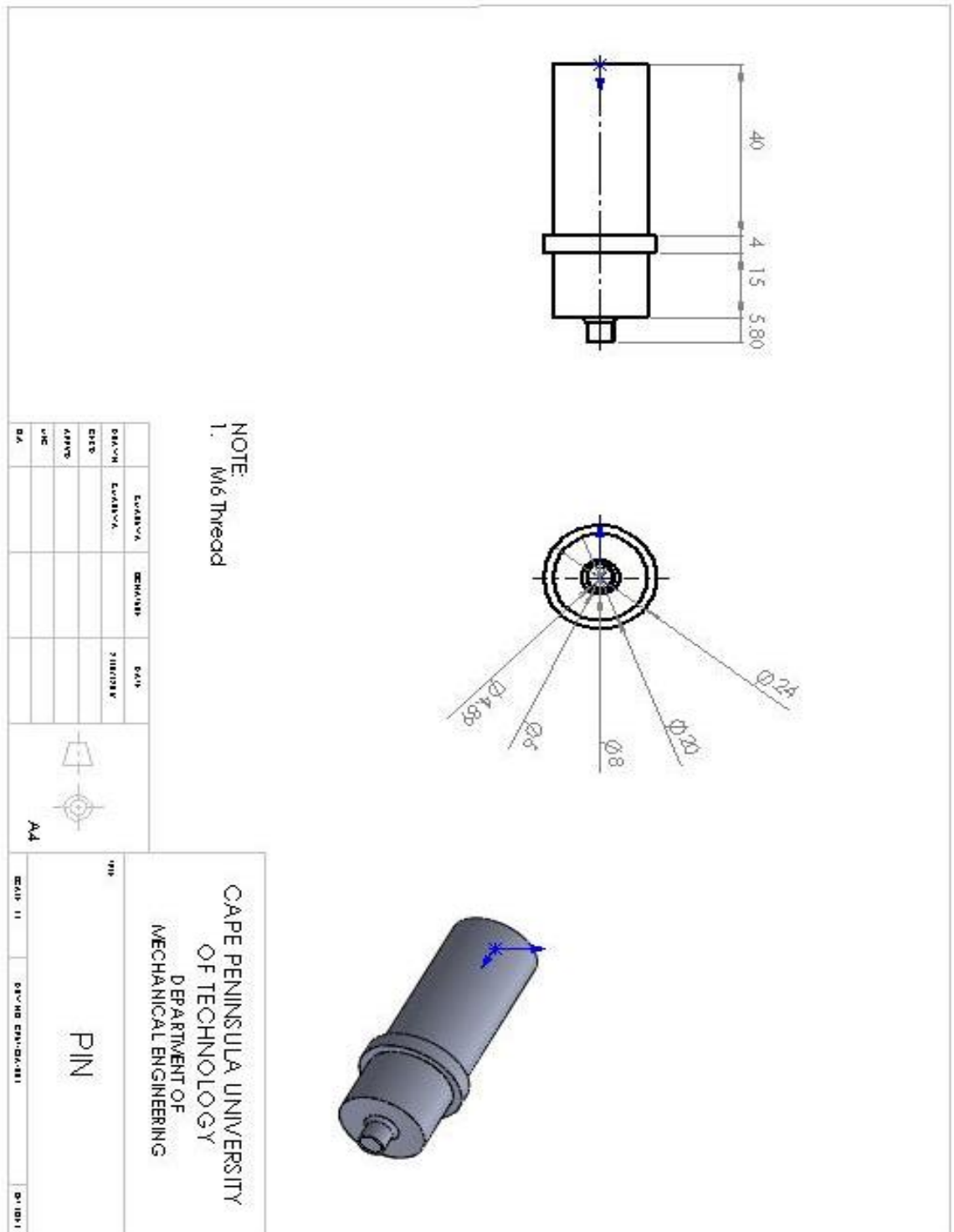


Figure B1: Pin.

APPENDIX C1

Tensile Test Specimen

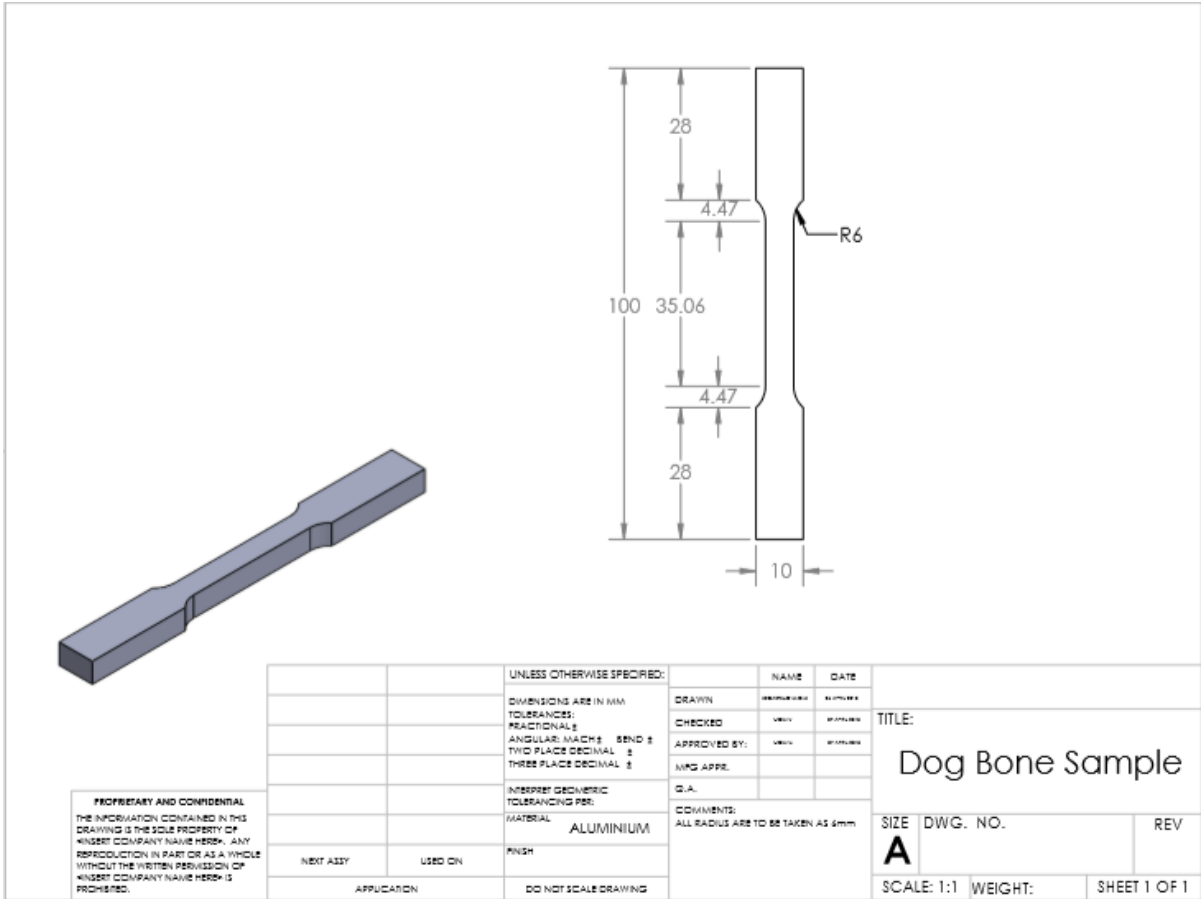
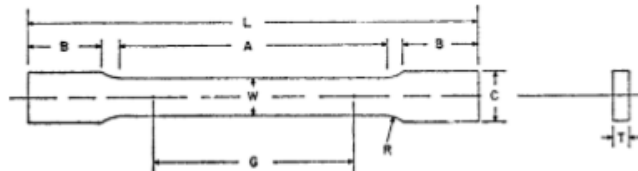


Figure C1: Dog Bone Specimen.

APPENDIX C2

ASTM E8 Standard

 E8/E8M - 13a



Dimensions	Standard Specimens		Subsize Specimen
	Plate-Type, 40 mm [1.500 in.] Wide	Sheet-Type, 12.5 mm [0.500 in.] Wide	6 mm [0.250 in.] Wide
	mm [in.]	mm [in.]	mm [in.]
G—Gauge length (Note 1 and Note 2)	200.0 ± 0.2 [8.00 ± 0.01]	50.0 ± 0.1 [2.000 ± 0.005]	25.0 ± 0.1 [1.000 ± 0.003]
W—Width (Note 3 and Note 4)	40.0 ± 2.0 [1.500 ± 0.125, -0.250]	12.5 ± 0.2 [0.500 ± 0.010]	6.0 ± 0.1 [0.250 ± 0.005]
T—Thickness (Note 5)		thickness of material	
R—Radius of fillet, min (Note 6)	25 [1]	12.5 [0.500]	6 [0.250]
L—Overall length, min (Note 2, Note 7, and Note 8)	450 [18]	200 [8]	100 [4]
A—Length of reduced section, min	225 [9]	57 [2.25]	32 [1.25]
B—Length of grip section, min (Note 9)	75 [3]	50 [2]	30 [1.25]
C—Width of grip section, approximate (Note 4 and Note 9)	50 [2]	20 [0.750]	10 [0.375]

Norm 1—For the 40 mm [1.500 in.] wide specimen, punch marks for measuring elongation after fracture shall be made on the flat or on the edge of the specimen and within the reduced section. Either a set of nine or more punch marks 25 mm [1 in.] apart, or one or more pairs of punch marks 200 mm [8 in.] apart may be used.

Norm 2—When elongation measurements of 40 mm [1.500 in.] wide specimens are not required, a minimum length of reduced section (A) of 75 mm [2.25 in.] may be used with all other dimensions similar to those of the plate-type specimen.

Norm 3—For the three sizes of specimens, the ends of the reduced section shall not differ in width by more than 0.10, 0.05 or 0.02 mm [0.004, 0.002 or 0.001 in.], respectively. Also, there may be a gradual decrease in width from the ends to the center, but the width at each end shall not be more than 1 % larger than the width at the center.

Norm 4—For each of the three sizes of specimens, narrower widths (W and C) may be used when necessary. In such cases the width of the reduced section should be as large as the width of the material being tested permits; however, unless stated specifically, the requirements for elongation in a product specification shall not apply when these narrower specimens are used.

Norm 5—The dimension T is the thickness of the test specimen as provided for in the applicable material specifications. Minimum thickness of 40 mm [1.500 in.] wide specimens shall be 5 mm [0.188 in.]. Maximum thickness of 12.5 and 6 mm [0.500 and 0.250 in.] wide specimens shall be 19 and 6 mm [0.750 and 0.250 in.], respectively.

Norm 6—For the 40 mm [1.500 in.] wide specimen, a 13 mm [0.500 in.] minimum radius at the ends of the reduced section is permitted for steel specimens under 690 MPa [100 000 psi] in tensile strength when a profile cutter is used to machine the reduced section.

Norm 7—The dimension shown is suggested as a minimum. In determining the minimum length, the grips must not extend in to the transition section between Dimensions A and B, see Note 9.

Norm 8—To aid in obtaining axial force application during testing of 6-mm [0.250-in.] wide specimens, the overall length should be as large as the material will permit, up to 200 mm [8.00 in.].

Norm 9—It is desirable, if possible, to make the length of the grip section large enough to allow the specimen to extend into the grips a distance equal to two thirds or more of the length of the grips. If the thickness of 12.5 mm [0.500-in.] wide specimens is over 10 mm [0.375 in.], longer grips and correspondingly longer grip sections of the specimen may be necessary to prevent failure in the grip section.

Norm 10—For the three sizes of specimens, the ends of the specimen shall be symmetrical in width with the center line of the reduced section within 2.5, 1.25 and 0.13 mm [0.10, 0.05 and 0.005 in.], respectively. However, for referee testing and when required by product specifications, the ends of the 12.5 mm [0.500 in.] wide specimen shall be symmetrical within 0.2 mm [0.01 in.].

Norm 11—For each specimen type, the radii of all fillets shall be equal to each other within a tolerance of 1.25 mm [0.05 in.], and the centers of curvature of the two fillets at a particular end shall be located across from each other (on a line perpendicular to the centerline) within a tolerance of 2.5 mm [0.10 in.].

Norm 12—Specimens with sides parallel throughout their length are permitted, except for referee testing, provided: (a) the above tolerances are used; (b) an adequate number of marks are provided for determination of elongation; and (c) when yield strength is determined, a suitable extensometer is used. If the fracture occurs at a distance of less than 2 W from the edge of the gripping device, the tensile properties determined may not be representative of the material. In acceptance testing, if the properties meet the minimum requirements specified, no further testing is required, but if they are less than the minimum requirements, discard the test and retest.

FIG. 1 Rectangular Tension Test Specimens

APPENDIX D

ASTM E290-14



Designation: E290 – 14

Standard Test Methods for Bend Testing of Material for Ductility¹

This standard is issued under the fixed designation E290; the number immediately following the designation indicates the year of original adoption or, in the case of revision, the year of last revision. A number in parentheses indicates the year of last reapproval. A superscript epsilon (ϵ) indicates an editorial change since the last revision or reapproval.

This standard has been approved for use by agencies of the U.S. Department of Defense.

1. Scope*

1.1 These test methods cover bend testing for ductility of materials. Included in the procedures are four conditions of constraint on the bent portion of the specimen; a guided-bend test using a mandrel or plunger of defined dimensions to force the mid-length of the specimen between two supports separated by a defined space; a semi-guided bend test in which the specimen is bent, while in contact with a mandrel, through a specified angle or to a specified inside radius (r) of curvature, measured while under the bending force; a free-bend test in which the ends of the specimen are brought toward each other, but in which no transverse force is applied to the bend itself and there is no contact of the concave inside surface of the bend with other material; a bend and flatten test, in which a transverse force is applied to the bend such that the legs make contact with each other over the length of the specimen.

1.2 After bending, the convex surface of the bend is examined for evidence of a crack or surface irregularities. If the specimen fractures, the material has failed the test. When complete fracture does not occur, the criterion for failure is the number and size of cracks or surface irregularities visible to the unaided eye occurring on the convex surface of the specimen after bending, as specified by the product standard. Any cracks within one thickness of the edge of the specimen are not considered a bend test failure. Cracks occurring in the corners of the bent portion shall not be considered significant unless they exceed the size specified for corner cracks in the product standard.

1.3 The values stated in SI units are to be regarded as standard. Inch-pound values given in parentheses were used in establishing test parameters and are for information only.

1.4 *This standard does not purport to address all of the safety concerns, if any, associated with its use. It is the responsibility of the user of this standard to establish appro-*

priate safety and health practices and determine the applicability of regulatory limitations prior to use.

2. Referenced Documents

2.1 *ASTM Standards:*²

E6 Terminology Relating to Methods of Mechanical Testing

E8/E8M Test Methods for Tension Testing of Metallic Materials

E18 Test Methods for Rockwell Hardness of Metallic Materials

E190 Test Method for Guided Bend Test for Ductility of Welds

3. Summary of Test Methods

3.1 Four methods for ductility testing employing bending are included in these test methods. Three methods have subgroups with specific procedures.

3.1.1 *Guided Bend:*

3.1.1.1 Guided Bend, No Die,

3.1.1.2 Guided Bend, U-Bend,

3.1.1.3 Guided Bend, V-Bend,

3.1.1.4 Guided Bend, V-Bend for cold rolled sheet,

3.1.2 *Semi-guided Bend:*

3.1.2.1 *Arrangement A*, specimen held at one end.

3.1.2.2 *Arrangement B*, for thin material.

3.1.2.3 *Arrangement C*, mandrel contact force in the bend.

3.1.3 *Free-Bend:*

3.1.3.1 *Type 1*, 180° bend.

3.1.3.2 *Type 2*, bend flat on itself.

3.1.4 *Bend and Flatten:*

3.2 A guided-bend test for ductility of welds is described in Method E190 and may be used for flat-rolled materials when specified by the product standard. The essential features of this bending method are employed in 3.1.1.2, Guided Bend, U-Bend.

3.3 Bend tests are made in one of two directions relative to the principal working direction employed in production processing of the material.

¹ This test method is under the jurisdiction of ASTM Committee E28 on Mechanical Testing and is the direct responsibility of Subcommittee E28.02 on Ductility and Formability.

Current edition approved May 1, 2014. Published September 2014. Originally approved in 1966. Last previous edition approved in 2013 as E290 – 13. DOI: 10.1520/E0290-14.

² For referenced ASTM standards, visit the ASTM website, www.astm.org, or contact ASTM Customer Service at service@astm.org. For *Annual Book of ASTM Standards* volume information, refer to the standard's Document Summary page on the ASTM website.

*A Summary of Changes section appears at the end of this standard

Copyright © ASTM International, 100 Barr Harbor Drive, PO Box C700, West Conshohocken, PA 19428-2999, United States

Copyright by ASTM Int'l (all rights reserved); Mon May 4 05:58:03 EDT 2015 1

Downloaded/printed by

Liverpool Univ (Liverpool Univ) pursuant to License Agreement. No further reproductions authorized.



Note 1—Arrow indicates direction of processing.
FIG. 1 Longitudinal Bend Test



Note 1—Arrow indicates direction of processing.
FIG. 2 Transverse Bend Test

3.3.3 Thin sheet products are generally produced by reducing the thickness of stock in rolling mills and from this the term rolling direction is used to identify the principal processing direction. Similarly, a product produced in coil form may have the processing direction referred to as the coiling direction.

3.4 The location of the force application to the specimen relative to the bend itself and the amount of bending differentiate the four methods of bending covered in these test methods. The two semi-guided-bend test procedures provide radiused surfaces over which the bend is formed. The results obtained by different test procedures may not be the same, especially for material with a tendency to crack or fracture.

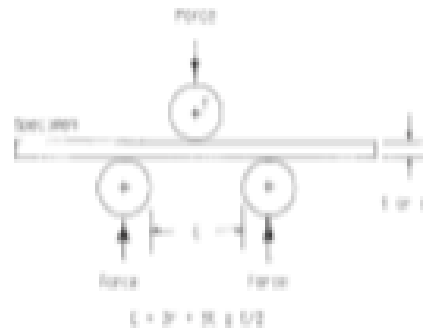
3.5 The test is completed when the designated angle of bend, or other specified condition, has been reached.

3.5.1 If a defined amount of cracking is permitted by the product standard, the convex surface of the bend region is examined for cracks and surface irregularities.

3.5.2 Surface irregularities, such as orange peel, loss of coating adherence, or imperfections resulting from the bend, shall be noted as required by the product specification.

3.6 **Guided-Bend**—The guided-bend test is made by supporting the specimen on pins, rollers, or radiused flats near each end and applying a force through a pin, mandrel, or plunger midway between two supports, as shown schematically in Fig. 3, until the desired bend is formed. No force is applied directly to the outer face of the bend.

3.6.1 The radii of the plunger and of the two supports shall be defined in the product specification or related to the thickness (t) of the specimen being tested. A clearance of three times thickness with a tolerance of one half thickness shall be provided between the pins, plunger, and specimen in the initial bend fixture.



Note 1— C = distance between lower supports,
 r = radius of the end of the mandrel or plunger,
 t = sheet specimen thickness,
 d = round specimen diameter, and
 w = sheet specimen width.

FIG. 3 Schematic Fixture for the Guided-Bend Test

3.6.1.1 The distance between supports (C) shall be three thicknesses plus twice the plunger radius, with a tolerance of one-half thickness, as shown in Fig. 3.

3.6.2 The surfaces of the supports and plunger shall be hardened to between 20 and 30 HRC. Refer to Method E 18.

3.6.3 The supports can be fixed or free to rotate. A lubricant may be applied to the supports and plunger.

3.6.4 The width of the guided-bend fixture, including the supports and plunger, shall be such that the specimen is subject to the bending force across its width (w) during bending.

3.6.5 When the thickness or strength of the specimen, or capacity of the guided-bend test fixture (shown in Fig. 3) does not produce the required amount of bending, the specimen can be removed from the fixture and the bend completed by applying force against the ends of the specimen, as shown schematically in Fig. 4. A spacer with a thickness equal to twice the required bend radius is inserted at the location of the bend. The edges at the ends shall be constrained so the specimen cannot eject from the fixture under the bending force.

3.6.6 Surface cracks and imperfections resulting from the bend shall be evaluated and reported.

3.7 **Semi-guided Bend**—The semi-guided-bend test employs a constraining force on the inside of the bend during the

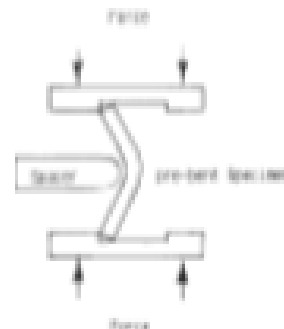
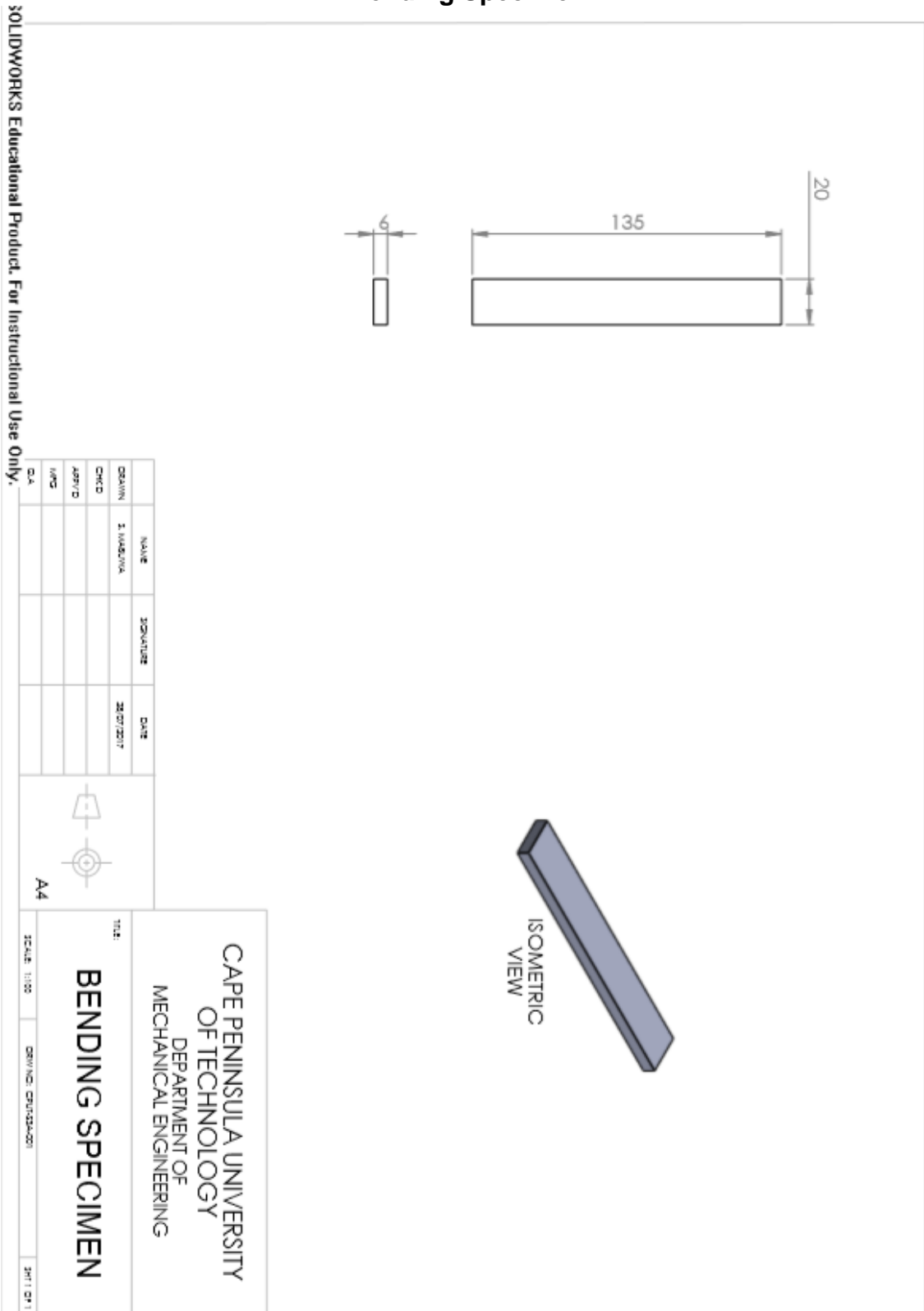


FIG. 4 Schematic Fixture for Completing the Guided-Bend Test Started as Shown in Fig. 3

APPENDIX D2

Bending Specimen



SOLIDWORKS Educational Product. For Instructional Use Only.

Figure D2: Bending Specimen.

APPENDIX E

Hardness Test Specimen

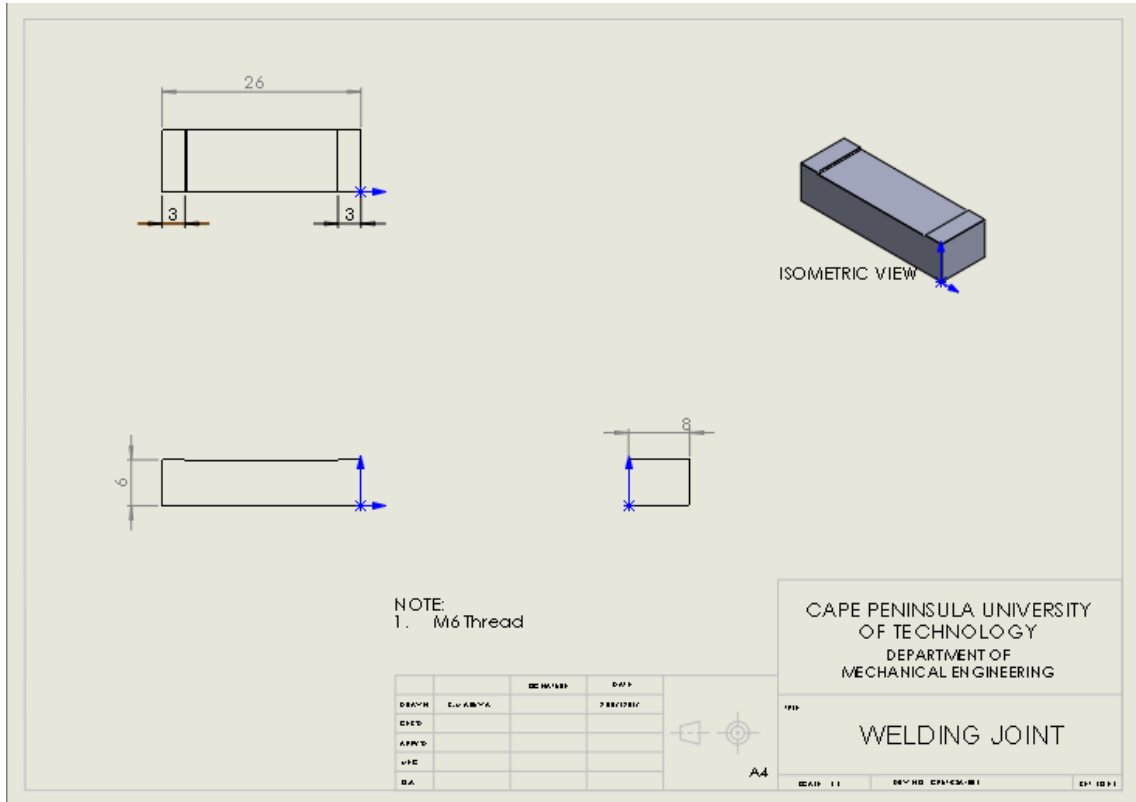


Figure E1: Welding Joint.

APPENDIX F
SAMPLE OF CALCULATIONS

Maximum Flexural Stress

$$\sigma = \frac{3FL}{2bd^2}$$

FSW (Root):

$$\sigma = \frac{3 \times 0.09 \times 2957}{2 \times 0.02 \times (0.006)^2}$$
$$\sigma = 554.4MPa$$

FSW (Face):

$$\sigma = \frac{3 \times 0.09 \times 3662}{2 \times 0.02 \times (0.006)^2}$$
$$\sigma = 686.625MPa$$

FSP-FSW (Face):

$$\sigma = \frac{3 \times 0.09 \times 2957}{2 \times 0.02 \times (0.006)^2}$$
$$\sigma = 759.75MPa$$

FSP-FSW (Root):

$$\sigma = \frac{3 \times 0.09 \times 3460}{2 \times 0.02 \times (0.006)^2}$$
$$\sigma = 648.75MPa$$

TIG (Face):

$$\sigma = \frac{3 \times 0.09 \times 1603}{2 \times 0.02 \times (0.006)^2}$$
$$\sigma = 300.563MPa$$

TIG (Root):

$$\sigma = \frac{3 \times 0.09 \times 2047}{2 \times 0.02 \times (0.006)^2}$$
$$\sigma = 383.813MPa$$

FSP-TIG (Face):

$$\sigma = \frac{3 \times 0.09 \times 3053}{2 \times 0.02 \times (0.006)^2}$$
$$\sigma = 572.438MPa$$

FSP-TIG (Root):

$$\sigma = \frac{3 \times 0.09 \times 2673}{2 \times 0.02 \times (0.006)^2}$$

$$\sigma = 501.188MPa$$

Strain and Percentage Elongation

$$\varepsilon = \frac{L2 - L1}{L1}$$
$$\% = \frac{\Delta L}{L} \times 100$$

FSW:

$$\varepsilon_1 = \frac{41.46 - 35.06}{35.06}$$
$$\varepsilon = 0.1711$$

$$\%E = 0.1711 \times 100$$
$$\%E = 17.11\%$$

$$\varepsilon_2 = \frac{6.5}{35.06}$$
$$\varepsilon = 0.1854$$
$$\%E = 18.54\%$$

$$\varepsilon_3 = \frac{5.8}{35.06}$$
$$\varepsilon = 0.1654$$
$$\%E = 16.54$$

Maximum Shear Stress

$$\tau = \frac{3F}{4bd}$$

FSW (Face):

$$\tau = \frac{3 \times 3662}{2 \times 0.02 \times 0.006}$$
$$\tau = 45.775MPa$$

FSW (Root):

$$\tau = \frac{3 \times 2957}{2 \times 0.02 \times 0.006}$$
$$\tau = 36.963MPa$$

FSP-FSW (Face):

$$\tau = \frac{3 \times 4052}{2 \times 0.02 \times 0.006}$$
$$\tau = 50.65MPa$$

FSP-FSW (Root):

$$\tau = \frac{3 \times 3460}{2 \times 0.02 \times 0.006}$$
$$\tau = 43.25MPa$$

TIG (Face):

$$\tau = \frac{3 \times 1603}{2 \times 0.02 \times 0.006}$$
$$\tau = 20.038MPa$$

TIG (Root):

$$\tau = \frac{3 \times 2047}{2 \times 0.02 \times 0.006}$$
$$\tau = 25.588MPa$$

FSP-TIG (Face):

$$\tau = \frac{3 \times 3053}{2 \times 0.02 \times 0.006}$$
$$\tau = 38.163MPa$$

Tensile Test Calculations

Ultimate Tensile Stress

$$\sigma = \frac{F}{A}$$

FSW:

$$\sigma_1 = \frac{9435}{0.006 \times 0.006}$$
$$\sigma_1 = 262.083MPa$$

$$\sigma_2 = \frac{9315}{0.006 \times 0.006}$$
$$\sigma_2 = 258.75MPa$$

$$\sigma_3 = \frac{9245}{0.006 \times 0.006}$$
$$\sigma_3 = 256.806MPa$$

FSP-FSW:

$$\sigma_1 = \frac{10297}{0.006 \times 0.006}$$
$$\sigma_1 = 286.028MPa$$

$$\sigma_2 = \frac{10911}{0.006 \times 0.006}$$
$$\sigma_2 = 303.083MPa$$

$$\sigma_3 = \frac{10798}{0.006 \times 0.006}$$
$$\sigma_3 = 299.944MPa$$

TIG:

$$\sigma_1 = \frac{1657}{0.006 \times 0.006}$$
$$\sigma_2 = 46.028MPa$$

$$\sigma_2 = \frac{5535}{0.006 \times 0.006}$$
$$\sigma_2 = 153.75MPa$$

$$\sigma_3 = \frac{4818}{0.006 \times 0.006}$$
$$\sigma_3 = 133.833MPa$$

FSP-TIG:

$$\sigma_1 = \frac{6722}{0.006 \times 0.006}$$

$$\sigma_1 = 186.822 \text{ MPa}$$

$$\sigma_2 = \frac{6198}{0.006 \times 0.006}$$

$$\sigma_2 = 172.167 \text{ MPa}$$

$$\sigma_3 = \frac{8997}{0.006 \times 0.006}$$

$$\sigma_3 = 249.917 \text{ MPa}$$

Strain and Percentage Elongation

$$\varepsilon = \frac{L_2 - L_1}{L_1}$$

$$\% = \frac{\Delta L}{L} \times 100$$

FSW:

$$\varepsilon_1 = \frac{41.46 - 35.06}{35.06}$$

$$\varepsilon = 0.1711$$

$$\%E = 0.1711 \times 100$$

$$\%E = 17.11\%$$

$$\varepsilon_2 = \frac{6.5}{35.06}$$

$$\varepsilon = 0.1854$$

$$\%E = 18.54\%$$

$$\varepsilon_3 = \frac{5.8}{35.06}$$

$$\varepsilon = 0.1654$$

$$\%E = 16.54\%$$

FSP – FSW:

$$\varepsilon_1 = \frac{8.6}{35.06}$$

$$\varepsilon_1 = 0.2453$$

$$\%E = 24.53\%$$

$$\varepsilon_2 = \frac{10.2}{35.06}$$

$$\varepsilon_2 = 0.2909$$

$$\%E = 29.09\%$$

$$\varepsilon_3 = \frac{10.7}{35.06}$$

$$\varepsilon_3 = 0.3052$$

$$\%E = 30.52\%$$

TIG:

$$\varepsilon_1 = \frac{2.3}{35.06}$$

$$\varepsilon_1 = 0.0656$$

$$\%E = 6.56\%$$

$$\varepsilon_2 = \frac{3.3}{35.06}$$

$$\varepsilon_2 = 0.0941$$

$$\%E = 9.41\%$$

$$\varepsilon_3 = \frac{3}{35.06}$$

$$\varepsilon_3 = 0.0856$$

$$\%E = 8.56\%$$

FSP-TIG:

$$\varepsilon_1 = \frac{5.6}{35.06}$$

$$\varepsilon_1 = 0.1597$$

$$\%E = 15.97\%$$

$$\varepsilon_2 = \frac{4.2}{35.06}$$

$$\varepsilon_2 = 0.1200$$

$$\%E = 12\%$$

$$\varepsilon_3 = \frac{8}{35.06}$$

$$\varepsilon_3 = 0.2286$$

$$\%E = 22.56\%$$

Yield Stress

$$\sigma = \frac{F}{A}$$

FSW:

$$\sigma_1 = \frac{6283}{0.006 \times 0.006}$$

$$\sigma_1 = 174.528 \text{ MPa}$$

$$\sigma_2 = \frac{3838}{0.006 \times 0.006}$$

$$\sigma_2 = 162.167MPa$$

$$\sigma_3 = \frac{6475}{0.006 \times 0.006}$$
$$\sigma_3 = 179.861MPa$$

FSP-FSW:

$$\sigma_1 = \frac{5030}{0.006 \times 0.006}$$
$$\sigma_1 = 139.722MPa$$

$$\sigma_2 = \frac{5645}{0.006 \times 0.006}$$
$$\sigma_2 = 156.806MPa$$

$$\sigma_3 = \frac{4270}{0.006 \times 0.006}$$
$$\sigma_3 = 118.611MPa$$

TIG:

$$\sigma_1 = \frac{1376}{0.006 \times 0.006}$$
$$\sigma_1 = 38.222MPa$$

$$\sigma_2 = \frac{2452}{0.006 \times 0.006}$$
$$\sigma_2 = 68.11MPa$$

$$\sigma_3 = \frac{1913}{0.006 \times 0.006}$$
$$\sigma_3 = 53.139MPa$$

FSP-TIG:

$$\sigma_1 = \frac{3363}{0.006 \times 0.006}$$
$$\sigma_1 = 93.42MPa$$

$$\sigma_2 = \frac{4395}{0.006 \times 0.006}$$
$$\sigma_2 = 122.08MPa$$

$$\sigma_3 = \frac{6250}{0.006 \times 0.006}$$
$$\sigma_3 = 173.611MPa$$